DNA damage and the activation of the p53 pathway mediate alterations in metabolic and secretory functions of adipocytes Running title: DNA damage and p53 in obese adipocytes

Bastien Vergoni, Pierre-Jean Cornejo, Jérôme Gilleron, Mansour Dedjani, Franck Ceppo, Arnaud Jacquel, Gwennaelle Bouget, Clémence Ginet, Teresa Gonzalez, Julie Maillet, et al.

DNA damage and the activation of the p53 pathway mediate alterations in metabolic and secretory functions of adipocytes

Bastien Vergoni[1,2*], Pierre-Jean Cornejo[1,2*], Jérôme Gilleron [1,2], Mansour Dedjani [1,2], Franck Ceppo[1,2], Arnaud Jacquel[3,2], Gwennaelle Bouget[1,2], Clémence Ginet[1,2], Teresa Gonzalez [1,2,4], Julie Maillet[5,6,7], Véronique Dhennin[5,6,7], Marie Verbanck[5,6,7], Patrick Auberger[3,2], Philippe Froguel[5,6,7,8], Jean-François Tanti[1,2,#], Mireille Cormont[1,2,#]

[1]INSERM, UMR 1065, C3M, Team 7 "Molecular and Cellular Physiopathology of Obesity and Diabetes", F-06204 Nice, France

[2]Université de Nice Sophia Antipolis, C3M, U1065, F-06204, Nice, France

[3]INSERM, UMR 1065, C3M, Team 2 "Cell Death, Differentiation and Cancer", F-06204 Nice, France

[4]INSERM, UMR1062, Nutrition, Obesity and Risk of Thrombosis, F-13385, Marseille, France

[5]CNRS, UMR8199, Lille Pasteur Institute, F-59000, Lille, France

[6]Lille University, Lille, France

[7]European Genomic Institute for Diabetes (EGID), Lille, France

[8]Department of Genomics of Common Disease, School of Public Health, Imperial College London, Hammersmith Hospital, London, UK

* Bastien Vergoni and Pierre-Jean Cornejo equally contributed to this study

Jean-François Tanti and Mireille Cormont are co-senior authors

Corresponding author:

Mireille Cormont, INSERM U1065, Centre Méditerranéen de Médecine Moléculaire (C3M), 151, route de St Antoine de Ginestière, BP 2 3194, 06204 Nice cedex 3, France.

Email: cormont@unice.fr , Phone number: +33 4 89 06 42 34, Fax number: +33 4 89 06 42 21

Running title: DNA damage and p53 in obese adipocytes

Diabetes Publish Ahead of Print, published online July 7, 2016

Abstract word count: 198; **Main text word count**: 3997

Number of figures: 8, **Supplemental Tables:** 2, **Supplemental Figures:** 6

Abstract

Activation of the p53 pathway in adipose tissue contributes to insulin resistance associated with obesity. However, the mechanisms of p53 activation and the impact on adipocyte functions are still elusive. Here we found a higher level of DNA oxidation and a reduction in telomere length in adipose tissue of high-fat diet mice and an increase in DNA damage and activation of the p53 pathway in adipocytes. Interestingly, hallmarks of chronic DNA damage are visible at the onset of obesity. Furthermore, treatment of lean mice with doxorubicin, a DNA damage-inducing drug, increased the expression of chemokines in adipose tissue and promoted its infiltration by pro-inflammatory macrophages and neutrophils together with adipocyte insulin resistance. In vitro, DNA damage in adipocytes increased chemokines expression and triggered the production of chemotactic factors for macrophages and neutrophils. Insulin signaling and effect on glucose uptake and Glut4 translocation were decreased while lipolysis was increased. These events were prevented by p53 inhibition whereas its activation by nutlin-3 reproduced the DNA damage-induced adverse effects. This study reveals that DNA damage in obese adipocyte could trigger p53-dependent signals involved in alteration of adipocyte metabolism and secretory function leading to adipose tissue inflammation, adipocyte dysfunction and insulin resistance.

Insulin resistance is associated with obesity and is a major risk factor for type 2 diabetes. Adipose tissue (AT) plays an important role in the glucose and lipid homeostasis (1,2) and AT dysfunction associated with obesity has emerged as a critical event for the development of insulin resistance. Both low grade inflammation and oxidative and hypoxic stresses develop in obese AT and are involved in the alteration of adipocyte functions (3-6). Therefore, activation of stress signaling pathways in adipocytes are critically involved in AT dysfunction and insulin resistance (7-10).

The tumor suppressor p53 has recently emerged as a novel regulator of metabolic homeostasis and adaptation to nutritional changes in different organs including AT (11-13). Thus, a role for the alterations of p53 activation has been proposed in metabolic diseases such as diabetes and obesity. Indeed, activation of p53 was reported in AT of genetically and high-fat/high-sugar obese mice (14,15) and it was shown that invalidation of p53 in adipocyte protects obese mice from insulin resistance and reduces AT inflammation (15). Conversely, p53 overexpression in adipocyte triggers insulin resistance and the expression of pro-inflammatory cytokines in the AT (15). Despite the significance of p53 activation in obese AT, its role in the alterations of adipocyte functions and the causes of its activation in obese AT are poorly understood.

The p53 pathway is a key effector of the DNA damage response (DDR) and is activated by several stressors that induce DNA lesions, the most deleterious one being DNA double-strand breaks (DSBs) (16). The oxidative stress occurring in AT of obese subjects is among the several possible stressors (4,15). We thus hypothesized that nuclear DNA damage in adipocytes triggers the activation of the p53 pathway leading to metabolic and endocrine dysfunctions in adipocyte and to systemic propagation of deleterious signals for insulin sensitivity.

Research Design and Methods

Cell culture

Human visceral preadipocytes from lean non-diabetic subjects (Biopredic, Rennes, France) and 3T3-L1 cells were differentiated into adipocytes as described (17,18). siRNA (Dharmacon) transfection was performed with INTERFERin^{TM} (Ozyme, St Quentin-en - Yvelines, France) as in (19). Raw 264.7 and Raw-blue^{TM} (InvivoGen) macrophages are maintained in DMEM-5% heat-inactivated FCS. Raw-blue^{TM} expressed the secreted embryonic alkaline phosphatase (SEAP) under the control of NF-κB and AP-1. Human mononucleated cells were isolated from blood using Ficoll Hypaque and monocytes were enriched and differentiated into M0 macrophages as in (20). Volunteers signed an informed consent according to the Declaration of Helsinki and recommendations of an independent scientific review board.

Animal studies

Male mice were purchased from Charles Rivers Laboratory (St-Aubin-lès-Elbeuf, France). *Ob/ob* and *ob/+* mice were used at 14 weeks of age. C57BL6/J mice were used for high-fat diets experiments (45 or 60 kcal% fat, SSNIFF, Soest, Germany) started at 7 weeks of age and continued for 2, 4, or 18 weeks (see Supplementary Table 1). 15 weeks-old C57BL/6J mice were injected for 42 h with doxorubicin (2mg/kg, Sigma-Aldrich) or 0.9 % NaCl for epiAT analysis. Intraperitoneal Glucose Tolerance Test (IPGTT) was performed as described (21) after starvation for 6 h. The Animal Care Committee of the Nice/Sophia-Antipolis University approved all studies.

Measurement of insulin signaling and metabolism in adipocytes

Insulin signaling, 2-[^{3}H]-deoxyglucose uptake, Glut4 translocation and lipogenesis on isolated adipocytes were determined as described (22). Glycerol content in the medium was

determined as read out of adipocyte lipolysis using the GPO-Trinder-colorimetric assay (Sigma).

Flow cytometry analysis of AT immune cells

The stroma vascular faction (SVF) cells obtained after epiAT treatment with collagenase (21) was incubated 15 min with Fc block, resuspended in dedicated buffer and stained for 30 min at 4 °C with fluorochrome-conjugated specific antibodies or control isotypes to quantify macrophages (F4/80 and CD11c), neutrophils (Lys6G and CD11b), T (CD3) or B (B220) lymphocytes. The labeling was analyzed by flow cytometry using a MACSQuant cytometer (Miltenyi) and the FlowJo software (TreeStar).

Immune cells chemotaxis and activation assays

Chemotaxis of RAW 264.7 and human M0 macrophages induced by adipocyte conditioned media (AdCM) was assessed by Boyden chambers assay (8-µm pores, BD Bioscience). Cells that are migrated at the filter lower face were labeled with Crystal Violet and counted in five randomly selected areas. For macrophage activation SEAP activity was quantified in the media of Raw-blue^{TM} cells. RNAs were prepared for the analysis of polarization marker expression. Human M0 polarization was determined by the quantification of the surface expression of M0, M1, and M2 markers as described (20).

To quantify neutrophil migration against AdCM, $2x10^5$ white blood cells were plated in the upper chamber of Boyden chambers (3-µm pores). 2 h later, cells in the lower chamber were labeled with FITC-coupled Lys6G and PE-coupled CD11b antibodies before flow cytometry analysis.

Immunofluorescence studies

Snap-frozen epiAT was embedded in Optimal-Cutting-Temperature medium. 15-µm sections were fixed in 4% PFA, incubated in 10 mM glycine, washed, and incubated in PBS/2%

BSA/0.1% Tween-20. Adipocytes from epiAT were isolated by collagenase digestion as described (21) and were fixed as above. The AT sections or isolated adipocytes were then incubated with the indicated antibodies and DAPI, washed, and mounted. Images were quantified using Motion-tracking software (23).

3Disco tissue clearing method (24) was adapted to AT. EpiAT was fixed in 3% PFA and successively washed in PBS containing either 0.2% Triton X-100, or 0.2% Triton X-100/20% DMSO, or 0.1% Tween-20/0.1% Triton X-100/0.1% deoxycholate/0.1% NP40/20% DMSO for 24 h each. EpiAT was then incubated overnight in PBS/0.2% Triton X-100/10% DMSO/0.3 M glycine and blocked by adding 6% BSA for 2 days. After 2 washes in PTwH (PBS/0.2% Tween-20/0.001% heparin), samples were incubated two days with FITC-labeled anti-γ-H2AX antibody, alexa647-phalloidin and DAPI in PTwH/5% DMSO/3% BSA and washed in PTwH for two extra days. The clearing was performed by successively using 50%, 75%, and 100% tetrahydrofuran 3h each time and finally with dibenzyl-ether for 2h before confocal acquisition and image analysis with FiJi software.

Microarray analysis

RNA was isolated from 3T3-L1 adipocytes using RNeasy Lipid Tissue Kit (Qiagen), quantified by a NanoDrop ND-1000, and their quality verified with an Agilent 2100. cRNA were prepared using TargetAmp Nano-g Biotin-aRNA Labeling for Illumina System (Epicentre) and hybridized to Illumina Mouse WG-6 v2.0 Beadarrays. Microarray data were normalized and analyzed using the Limma package of the R software (25). We performed a background correction using negative controls on the raw data, we applied a quantile normalization using positive controls followed by a log2 transformation, and we applied a 1% threshold on the detection p-values, which led to consider 13314 genes as expressed. We analyzed the variance (ANOVA) using the “eBayes” procedure of Limma and p-values were

corrected for multiple testing using Benjamini and Hochberg's method to control the false discovery rate with a 5% threshold.

ROS, DNA oxidation and Telomere length determination

ROS was quantified in 30-µm epiAT sections using DHE as described in (15) or in isolated adipocytes using the ROS-probe H2DCFDA (10µM). Adipocytes were recovered by centrifugation on dinonylphthalate and resuspended in H_2O_2 before fluorescence measurement. DNA was prepared from snap-frozen epiAT (DNeasy blood & tissue kit, Qiagen). 8-hydroxy-2-deoxyguanosine (8-OHdG) amounts were determined using EIA-dedicated kit (StressMarq Biosciences Inc) using manufacturer's recommendations. Quantitative-PCR was used that compares telomere repeat sequence copy number to single copy gene albumin.

Western Blotting and RT-qPCR

Cells were lysed and immunoblotting was performed as described (26) using indicated antibodies. RNA preparation and qRT-PCR were performed as described (26). Primers were from SABiosciences (Qiagen). The PCR data were analyzed with the comparative Ct (ΔΔCt) quantitation method.

Statistical analysis

Data are expressed as the mean $\pm$ SEM. Differences among groups were compared using ANOVA with post-hoc analysis for multiple comparisons and Mann and Whitney test or Student's *t* test when there were only two groups. Correlation analysis was done by Spearman test. Statistical analyses were performed using GraphPad PRISM 5 software, and the differences were considered significant when $P < 0.05$.

Results

The p53 pathway is activated in adipocytes from obese mice

The p21 mRNA level, a p53-target gene, was higher in epiAT and in the adipocyte fraction of the obese *ob/ob* and high-fat diet (HFD) fed mice compared to their lean counterparts (Fig. 1*A, B*). The p21 mRNA level in the adipocyte fraction from *ob/ob* and HFD-fed mice was positively correlated to whole body and fat pad weights and fasting glycemia (Supplementary Table 2). Expression of p53 and p21 proteins was higher in adipocytes from HFD-fed compared to normal chow diet (NCD) fed mice (Fig. 1*C*). Moreover, the number of adipocytes with a p21-positive nucleus was higher in HFD-fed mice compared to NCD-fed mice (61.7 % $\pm$ 5.50 *vs* 19.9 % $\pm$ 4.04, respectively, $p < 0.01$, Fig. 1*D*). This supports an activation of the p53 pathway in mature obese adipocytes.

A high-fat diet causes DNA damage in adipocytes which occurs early upon obesity onset

A main cause for p53 activation is DNA damage such as telomere shortening and/or DNA double-strand breaks (DSBs) themselves caused by ROS-induced DNA oxidation. We found a 1.5 fold increase in 8-OHdG, a marker of oxidative DNA damage (27), in the epiAT from HFD-fed mice for 18 weeks (Fig. *1E*) which positively correlated with p21 expression (Fig *1F*) suggesting a link between DNA oxidation and p53 activation. We quantified the number of adipocytes with nuclear foci containing phosphorylated histone H2AX (γ-H2AX) which positively correlates with DNA damage. The proportion of adipocytes with no γ-H2AX foci, meaning without DNA damage, was lower in HFD-fed compared to NCD-fed mice (6% *vs* 12%, respectively) (point 0 in Fig. 1*I*). Furthermore, the proportion of adipocytes with high numbers of γ-H2AX foci per nucleus was increased in adipocytes from HFD-fed mice (representative image in Fig. 1*H* and quantification of 80-120 adipocytes per group in Fig. 1*I*). Moreover, we found shortened telomeres in epiAT from HFD-fed mice (Fig. 1*G*) and

telomere length was inversely correlated to p21 expression, whole body and fat pad weights, and fasting glycemia (Supplementary Table 2).

We next asked whether adipocyte DNA damage was an early event upon the onset of obesity by studying mice after 2 and 4 weeks of HFD-feeding which increased body weight gain, epiAT weight and adipocyte size (Supplementary Fig. 1*F-H*). Using the 3Disco method, we imaged the whole epiAT and characterized cell types with DNA damage using γ-H2AX labeling. Two or four weeks of HFD increased by 2 to 3-fold respectively the number of adipocytes with γ-H2AX-positive nuclei (cyan color) (Fig. *2A, B*). ROS amounts were concomitantly increased both in epiAT and in adipocytes (Fig. 2*C*). DNA damage was also detected in non-adipocyte cells (white color in Fig. 2*A*). The expression of p53 protein and of p21 mRNA was increased together with the expression of $p16^{INK4A}$ and $p19^{ARF}$ mRNA encoded by the *CDKN2A* locus which are hallmarks of chronic DNA damage (Fig. *2D*) (28). Importantly, after 2 weeks of HFD, we did not observe features of insulin resistance of adipocytes since insulin-induced lipogenesis in isolated adipocytes (Fig. 2*E*) and epiAT expression of IRS1 and adiponectin mRNA was not different compared to NCD-fed mice while Glut4 mRNA level was increased (Fig. 2*F*). Leptin mRNA level was increased in agreement with the increase in epiAT weight and adipocyte diameter (Fig. 2*F,* Supplementary Fig. 1 *A*, *B*). Two weeks of HFD feeding did not markedly alter glucose homeostasis since IPGTT indicated similar glucose tolerance (Fig. 2*G*) with no difference in insulin secretion during IPGTT compared to NCD-fed mice (0.89 ng/ml $\pm$ 0.13 *vs* 0.84 ng/ml $\pm$ 0.15, respectively). Moreover, 2 weeks of HFD did not modify the insulin resistance index (HOMA-IR) (Fig. 2*H*) and the fasting and fed glycemia or insulinemia (Supplementary Fig. 1*C, D)*. By contrast, mice developed glucose intolerance after 4 weeks of HFD-feeding with a further increase in whole body and epiAT weights and adipocyte size as well as a trend toward a decrease in IRS1 mRNA (Supplementary Fig. 1*A, B, E-I*).

After two weeks of HFD, we found in epiAT a lower iNOS/Arg ratio, an up-regulation of the M2 marker CD206 mRNA, and of the chemokine CCL2 but we did not detect any significant differences in the number of F4/80$^+$CD11c$^-$ macrophages or of pro-inflammatory F4/80$^-$ CD11c$^+$ or F4/80$^+$CD11c$^+$ cells (Fig. 2*I*), neutrophils or T and B lymphocytes (Supplementary Fig. 1*K*, *L*). Furthermore, inflammatory gene expression in epiAT or circulating level of IL-6 and TNF-α did not significantly differ compared to NCD-fed mice (Fig. 2*I*). By contrast, infiltration of neutrophils in epiAT was observed after 4 weeks of HFD and was detectable until 18 weeks (Supplementary Fig. 1 *K, L*) with a further increase in CCL2 and IL-6 mRNA and a trend toward an increase in CD11c mRNA (Supplementary Fig. 1*J*).

These observations support that DNA damage and p53 activation occur very early during obesity development concomitantly to an increase in adipocyte ROS but before the insulin resistance of adipocyte, the inflammation of AT and the glucose intolerance.

DNA damage causes AT inflammation and adipocyte insulin resistance *in vivo*

We next assessed the impact of DNA damage on AT inflammation and adipocyte function by treating lean mice with short-term injection of the DNA-damaging drug doxorubicin. The weight of epiAT did not differ between control and doxorubicin-treated mice (377.0 mg $\pm$ 31.2 *vs* 348.3 mg $\pm$ 19.6, respectively) but doxorubicin treatment increased the amount of F4/80$^+$CD11c$^-$ and F4/80$^+$CD11c$^+$ macrophages as well as F4/80$^-$CD11c$^+$ dendritic-like cells in the epiAT (Fig. *3A*). Histological examination revealed an infiltration of polynuclear cells in epiAT of doxorubicin-treated mice consisting for 50% of Lys6G$^+$ neutrophils without difference in adipocyte size (Fig. *3B*). These changes in immune cells were associated with an increase in inflammatory markers such as p65-NFκB phosphorylation in the SVF (Fig. *3C* TNF-α, IL-1β, and IL-6 mRNA in epiAT, adipocytes, or SVF (Fig. *3D)* and with a decrease in anti-inflammatory marker CD206 mRNA with a trend toward a decrease of IL-10 mRNA (Fig. *3D*). As expected, p53 was activated in the epiAT and adipocytes of doxorubicin-treated

mice, as indicated by the increase in p21 (Fig. *3E*). Doxorubicin decreased Glut4 mRNA and protein, IRS1 and adiponectin mRNA (Fig. *3E, F*), and the PKB/Akt phosphorylation in adipocytes featuring insulin resistance of adipocytes (Fig. *3F*). Accordingly, insulin-induced lipogenesis was decreased in isolated adipocytes from doxorubicin-treated mice and circulating NEFA level was increased (Fig. *3F, G*). These changes in adipocyte functions and AT inflammation did not markedly impact on whole body glucose metabolism because the IPGGT and insulin secretion during this test were unchanged (Fig. 3*H*, *I*).

Adipocyte-mediated macrophage chemotaxis is increased by doxorubicin-induced DNA damage and p53 activation

Based on the above findings, we hypothesized that DNA damage and activation of p53 in adipocytes promote the secretion of chemotactic factors triggering immune cells infiltration in AT. We thus investigated *in vitro* the chemotaxis activity of conditioned media (AdCM) from adipocytes treated with doxorubicin to induce DNA damage or with nutlin-3 to activate p53 pathway. Features of DNA damage such as increased number of γ-H2AX foci and of p21 expression, stabilization and phosphorylation of p53, were observed in doxorubicin-treated 3T3-L1 adipocytes (Supplementary Fig. 2*A*-*C*). Nutlin-3, an inhibitor of the ubiquitin-ligase mdm2 involved in p53 degradation (29) also induced the stabilization and phosphorylation of p53 and the induction of p21 without inducing DNA damage (Supplementary Fig. *2A*-*C*). AdCM from doxorubicin- or nutlin-3-treated 3T3-L1 adipocytes did not increase the pro-inflammatory polarization of mouse RAW macrophages or human monocyte-derived macrophages (Fig. 4*A* and Supplementary Fig. 3*A, B*). Importantly, AdCM from doxorubicin- or nutlin-3-treated adipocytes exhibited a higher chemotactic activity toward mouse macrophages or human monocyte-derived macrophages compared to AdCM from control adipocytes (Fig. 4*B, C*). Compared to control medium or AdCM from control adipocytes, AdCM from doxorubicin or nutlin-3-treated adipocytes also exhibited a higher chemotactic

activity towards neutrophil, an effect which is similar or even greater (for doxorubicin treatment) than the neutrophil chemotactic factor fMLP (Fig. 4*D*).

Microarray analysis of 3T3-L1 adipocytes treated with doxorubicin or nutlin-3 revealed that among the expressed chemokines, eleven were deregulated in one or both experimental conditions (Fig. 5*A*). Analysis by qRT-PCR confirmed that doxorubicin and nutlin-3 increased the mRNA expression of CCL9 (a fibroblast and dendritic cells chemotactic protein), CXCL1 (a neutrophil chemotactic protein) and CCL2 while the expression of CCL7 mRNA, another monocytic chemotactic protein was increased by nutlin-3 only (Fig. 5*B, C*). Doxorubicin and nutlin-3 also induced the expression of IL-6. The silencing of p53 blocked the induction by nutlin-3 of all of these mRNAs (Fig.5*B*) and partly prevented their up-regulation in response to doxorubicin, except for CXCL1 (Fig. 5*C*). Since p53 silencing only partially reduced p53 expression and activation by doxorubicin (Supplementary Fig. 2*C*), we treated cells with both p53 siRNA and pifithrin-α, an inhibitor of p53 transcriptional activity. In this condition, CCL2/9, CXCL1, and IL-6 mRNA induction was prevented (Fig. 5*C*). Importantly, we found that the expression of mRNAs coding for CCL2/7/9 and CXCL1 was increased in epiAT from doxorubicin-treated, both in the adipocyte and SVF fractions for CCL2/7 and only in the adipocyte fraction for CCL9 and CXCL1 (Fig. 5*D*). We also examined the expression of these chemokines at the onset of obesity when DNA damage was observed in adipocytes. CCL2 mRNA level was increased after 2 weeks of HFD-feeding (Fig. 2*I*) and a trend toward an increase for CCL9 mRNA was observed (Fig. 5*E*). The mRNA levels of all of these chemokines were significantly increased after 4 weeks of HFD-feeding (Fig. 5*F* and Supplementary Fig. 1*J*).

DNA damage and p53 activation inhibit insulin signaling and insulin-induced glucose transport and increase lipolysis in adipocytes

We next assessed whether the insulin resistance of adipocytes from doxorubicin-treated mice (Fig. 3) was only the consequences of AT inflammation, or might also be due to an adipocyte cell-autonomous effect of DNA damage and p53 activation. Treatment of 3T3-L1 adipocytes with doxorubicin or nutlin-3 reduced insulin-induced glucose uptake (Fig. 6*A, B*) and Glut4 translocation (Fig. 6*E, F*) without changing Glut1 and Glut4 expression (Fig. 6*C*, *D*). Similar results were obtained in human adipocytes (Supplementary Fig. 4*A, B*). This effect was associated with a decrease in insulin signaling in 3T3-L1 and human adipocytes (Fig. 7*A*, *B* and Supplementary Fig. 4*C*, *D*). The insulin-induced PKB/Akt phosphorylation in 3T3-L1 adipocytes treated with doxorubicin or nutlin-3 was improved by p53 silencing which partially reduced p53 expression (Supplementary Fig. 5*A*) or by treatment with pifithrin-α (not shown) and fully restored when p53 expression and activity was reduced by using both p53 siRNA and pifithrin-α (Fig. 7*D, E* and supplementary Fig. 5*B*). It was unlikely that the deleterious effects of doxorubicin and nutlin-3 involved secretory factors since treatment of adipocytes with AdCM from doxorubicin- or nutlin-3-treated 3T3-L1 adipocytes did not alter insulin-induced PKB/Akt phosphorylation (Fig. 7*C*).

An increase in lipolysis contributes to AT inflammation and to the alteration in insulin sensitivity (30). We found that doxorubicin or nutlin-3 increased lipolysis in 3T3-L1 and human adipocytes as evidenced by an increase in glycerol release (Fig. 8*A, B* and Supplementary Fig. 4*E, F*). The p53 silencing in 3T3-L1 adipocytes decreased by 50 % the nutlin-3-induced lipolysis (Fig. 8*A*). The lipolytic effect of doxorubicin was modestly but significantly reduced by p53 silencing and markedly inhibited by using both p53 siRNA and pifithrin-α (Fig. 8*B*). Pifithrin-α alone inhibits by 63.7 % $\pm$ 6.8 and 34.8 % $\pm$ 3.3 nutlin-3- and doxorubicin-induced lipolysis, respectively.

To further explore the mechanisms of the lipolytic effect of DNA damage and p53 activation, we examined the expression of the lipolytic enzymes and/or of lipid droplet components.

Microarray analysis revealed that genes involved in the maintenance of the lipid droplet integrity and the repression of basal lipolysis such as PLIN1 (coding for perilipin 1) and CIDEC (31,32) were down-regulated in both doxorubicin- or nutlin-treated 3T3-L1 adipocytes (Fig. 8C). The protein level of perilipin 1 was decreased in adipocytes treated with doxorubicin or nutlin-3 (Fig. 8D).

Discussion

Previous studies have reported an up-regulation of the p53 pathway in AT of obese rodents and patients (14,15,33) but the causes of p53 activation in obese adipocytes and its consequences on adipocyte metabolism remain ill-defined. Here, we show with several image-based approaches an increased in DNA damage in adipocytes not only when obesity was established but early upon the onset of obesity before alterations in adipocyte insulin sensitivity and whole-body glucose homeostasis. In addition to adipocytes, other cell types that remain to be characterized also had DNA damage. Some of them aligned in branched actin-rich structures could be endothelial cells in which p53 was activated in obesity (34). Taking into account the high number of γ-H2AX foci per nuclei compared to telomere number in the adipocytes from mice with installed obesity, it is likely that both DSBs and telomere shortening occurred. DNA damage may thus contribute to p53 stabilization and p21 up-regulation we observed in adipocytes from HFD-fed mice. Of note, those adipocytes were not apoptotic possibly because the induction of p21 protected them from apoptosis (35).

What could be the cause of adipocyte DNA damage? DNA is sensitive to damage induced by oxidative stress and we indeed detected an increase in 8-OHdG level, the most common oxidative DNA lesions (36), in AT from obese mice. These oxidative DNA lesions may contribute to p53 activation in obese adipocyte because we found a positive correlation between 8-OHdG amounts and the expression of the p53-target p21. In installed obesity, both

adipocytes and pro-inflammatory macrophages may contribute to the increase in ROS production (37,38) that could induce DNA damage in adipocytes and other AT cells. However, we also observed DNA damage and ROS in adipocytes at the onset of obesity before any increase in pro-inflammatory macrophages or pro-inflammatory cytokines and before alterations in whole-body glucose homeostasis and adipocyte insulin sensitivity. This increase in ROS may induce DNA damage and consequently activation of the DDR known to induce innate inflammatory response (39) and thus could be causal factors in obese AT inflammation and adipocyte dysfunctions.

Such a link between adipocyte DNA damage, AT inflammation and insulin resistance of adipocytes is supported by the increased amount of pro-inflammatory immune cells in the AT and the adipocyte insulin resistance of lean mice treated with the DNA damage-inducing drug doxorubicin. Our data argue that these changes in AT immune cells are the consequence of p53-dependent secretion of chemokines induced by DNA damage in the adipocytes. Importantly, the changes in immune cells populations and in chemokine expression in AT of doxorubicin-treated mice is at least qualitatively consistent with those described in obesity (40,41). Therefore, DNA damage in adipocyte may trigger macrophages and neutrophils recruitment within AT through the p53-dependent production of several chemokines. Because the secretome from adipocytes treated *in vitro* with doxorubicin did not promote macrophage polarization, the increase in pro-inflammatory macrophages in AT from doxorubicin-treated mice would either be due to DNA damage in other cell types or to the vicious cycle that takes place between adipocytes and macrophages leading to macrophage activation (42). Also, other adipocyte p53-dependent mechanisms could contribute to AT inflammation during obesity (43).

Hence, DNA damage by increasing AT inflammation may promote adipocyte insulin resistance and dysfunction. However, DNA damage may also trigger adipocyte insulin

resistance independently of AT inflammation since inducing DNA damage in cultured adipocyte decreased insulin signaling and uptake of glucose and increased lipolysis. This is not due to a paracrine action of adipocyte-secreted factors. It is thus plausible that the DDR, mainly through p53 activation, promotes transcription of proteins down-regulating insulin signaling that remains to be identified but it was unlikely that MAP kinases were involved because they were not activated in our settings (data not shown). Based on our findings, it is tempting to speculate that DNA damage by altering adipocyte functions contributes to systemic insulin resistance. Indeed, by decreasing glucose flux, DNA damage may reduce *de novo* lipogenesis and such decrease is associated with reduced insulin sensitivity (44-46) whereas DNA damage increases lipolysis which is positively correlated with insulin resistance (30).

In summary, our study shows that DNA damage occurs early in the adipocytes at the onset of obesity and before the development of AT inflammation and adipocyte insulin resistance. DNA damage in adipocyte may be thus causal in the dysfunction and inflammation of AT (Supplementary Fig. 6). Pharmacological or nutritional strategies preventing DNA damage in adipocytes may thus be beneficial for the metabolic complications of obesity.

Author contributions

B.V. and P.-J.C. designed and performed most of the experiments, analyzed the data and reviewed the manuscript. M.D., C.G., T.G. performed experiments. F.C. performed RAW-Blue macrophage experiments. A.J. and P.A. were involved in the design and the realization of the experiments with human-derived macrophages. G.B. performed the chemotaxis assay with neutrophils. P.F., J.M., M.V., V.D. generated and analyzed microarray data. J.G. was involved in researched data and contributed to discussion and reviewed/edited manuscript. J.-F.T. contributed to data analysis, the discussion and wrote the manuscript. M.C. designed the study, was involved in data analysis and wrote the manuscript. M.C. is the guarantor of this work and, as such, had full access to all the data in the study and takes full responsibility for the integrity of the data, the accuracy of the data analysis, and for the decision to submit for publication.

Acknowledgments

We thank the animal facility staff for animal care and breeding as well as Damien Alcor at the head of the cell imaging core facility (INSERM U1065, C3M, Nice, France). We thank Pr Marino Zerial and Dr Yannis Lalaiszidis (Max Planck Institute of Cell Biology and Genetics, Dresden) for the free access to the Motion tracking software developed in Pr Zerial's laboratory.

Funding

This work was supported by INSERM, the Université de Nice Sophia Antipolis and by grants from the European Foundation for the Study of Diabetes (EFSD/Lilly), SFD-Abbott, Aviesan/AstraZeneca (Diabetes and the vessel wall injury program) and the French National Research Agency (ANR) through the "Investments for the Future" LABEX SIGNALIFE (ANR-11-LABX-0028-01 grant). Light microscopy was performed on the C3M Imaging Core Facility (part of Microscopy and Imaging platform Côte d'Azur, MICA IBISA). The Nikon

A1R-FLIM microscope used for this study was funded thanks to Conseil Général Alpes-Maritimes (“Appel à Projets Santé”) and by Région PACA (“Appel à Projets Plateforme”). The UMR 8199 genotyping and expression plateforme (Lille, France) belongs to the 'Federation de Recherche' 3508 funded by LABEX EGID (European Genomics Institute for Diabetes; ANR-10-LABX-46) and by the ANR Equipex 2010 session (ANR-10-EQPX-07-01; 'LIGAN-PM'). The LIGAN-PM Genomics platform (Lille, France) is also supported by the FEDER and the Region Nord-Pas-de-Calais-Picardie. B.V. and P-J.C. were supported by the French Ministry of Education and Research. J.G. was supported by a fellowship from the “Fondation pour la Recherche Médicale”. F.C. was supported by a fellowship from INSERM/Région PACA/FEDER and by a grant from the Société Francophone du Diabète (SFD). G.B. was supported by the LABEX SIGNALIFE grant (ANR-11-LABX-0028-01). J.-F.T is an investigator of the Centre National de la Recherche Scientifique (CNRS).

Duality of Interest

The authors declare no conflict of interest.

References

1. Kahn BB, Flier JS. Obesity and insulin resistance. J Clin Invest 2000;106:473-481
2. Herman MA, Kahn BB. Glucose transport and sensing in the maintenance of glucose homeostasis and metabolic harmony. J Clin Invest. 2006;116:1767-1775
3. Hotamisligil GS. Inflammation and metabolic disorders. Nature 2006;444:860-867
4. Furukawa S, Fujita T, Shimabukuro M, Iwaki M, Yamada Y, Nakajima Y, Nakayama O, Makishima M, Matsuda M, Shimomura I. Increased oxidative stress in obesity and its impact on metabolic syndrome. J Clin Invest 2004;114:1752-1761
5. Houstis N, Rosen ED, Lander ES. Reactive oxygen species have a causal role in multiple forms of insulin resistance. Nature 2006;440:944-948
6. Trayhurn P. Hypoxia and adipocyte physiology: implications for adipose tissue dysfunction in obesity. Annu Rev Nutr 2014;34:207-236
7. Gregor MF, Hotamisligil GS. Inflammatory mechanisms in obesity. Annu Rev Immunol 2011;29:415-445
8. Bashan N, Kovsan J, Kachko I, Ovadia H, Rudich A. Positive and negative regulation of insulin signaling by reactive oxygen and nitrogen species. Physiol Rev 2009;89:27-71
9. Tanti J-F, Jager J. Cellular mechanisms of insulin resistance: role of stress-regulated serine kinases and insulin receptor substrate (IRS) serine phosphorylation. Curr Opin Pharmacol 2009;9:753-762
10. Regazzetti C, Peraldi P, Grémeaux T, Najem-Lendom R, Ben-Sahra I, Cormont M, Bost F, Le Marchand-Brustel Y, Tanti J-F, Giorgetti-Peraldi S. Hypoxia decreases insulin signaling pathways in adipocytes. Diabetes 2009;58:95-103
11. Hafsi H, Hainaut P. Redox control and interplay between p53 isoforms: role in the regulation of basal p53 levels, cell fate, and senescence. Antioxid Redox Signal 2011;15:155-1667
12. Hallenborg P, Feddersen S, Madsen L, Kristiansen K. The tumor suppresors pRB and p53 as regulators of adipocyte differentiation and function. Expert Opin Ther Targets 2009;13:235-246
13. Schupp M, Chen F, Briggs ER, Rao S, Pelzmann HJ, Pessentheiner AR, Bogner-Strauss JG, Lazar MA, Baldwin D, Prokesch A. Metabolite and transcriptome analysis during fasting suggest a role for p53-Ddit4 axis in major metabolic tissues. BMC Genomics 2013;14:758
14. Yahagi N, Shimano H, Matsuzaka T, Najima Y, Sekiya M, Nakagawa Y, Ide T, Tomita S, Okazaki H, Tamura Y, Iizuka Y, Ohashi K, Gotoda T, Nagai R, Kimura S, Ishibashi S, Osuga J-i, Yamada N. p53 activation in adipocytes of obese mice. J Biol Chem 2003;278:25395-25400
15. Minamino T, Orimo M, Shiminzu I, Kunieda T, Yokoyama M, Ito T, Nojima A, Nabetani A, Oike Y, Matsubara H, Ishikawa F, Komuro I. A crucial role for adipose tissue p53 in the regulation of insulin resistance. Nat Med 2009;15:1082-1087
16. Phillips ER, McKinnon PJ. DNA double-strand break repair and development. Oncogene 2007;26:7799-7808
17. Kaddai V, Jager J, Gonzalez T, Najem-Lendom R, Bonnafous S, Tran A, Le Marchand-Brustel Y, Gual P, Tanti J-F, Cormont M. Involvement of TNF-alpha in abnormal adipocyte and muscle sortilin expression in obese mice and humans. Diabetologia 2009;52:932-940
18. Jager J, Grémeaux T, Gonzalez T, Bonnafous S, Debard C, Laville M, Vidal H, Tran A, Gual P, Le Marchand-Brustel Y, Cormont M, Tanti J-F. Tpl2 kinase is upregulated in adipose tissue in obesity and may mediate interleukin-1beta and tumor necrosis factor-alpha effects on extracellular signal-regulated kinase activation and lipolysis. Diabetes 2010;59:61-70
19. Kaddai V, Gonzalez T, Keslair F, Grémeaux T, Bonnafous S, Gugenheim J, Tran A, Gual P, Le Marchand-Brustel Y, Cormont M. Rab4b is a small GTPase involved in the control of the glucose transporter GLUT4 localization in adipocyte. PLoS One 2009;e: 5257:
20. Obba S, Hizir Z, Boyer L, Selimoglu-Buet D, Pfeifer A, Michel G, Hamouda MA, Goncalves D, Cerezo M, Marchetti S, Rocchi S, Droin N, Cluzeau T, Robert G, Luciano F, Robaye B, Foretz M, Viollet B, Legros L, Solary E, Auberger P, Jacquel A. The PRKAA1/AMPKalpha1 pathway triggers autophagy during CSF1-induced human monocyte differentiation and is a potential target in CMML. Autophagy 2015;11:1114-1129

21. Jager J, Corcelle V, Gremeaux T, Laurent K, Waget A, Pages G, Binetruy B, Le Marchand-Brustel Y, Burcelin R, Bost F, Tanti JF. Deficiency in the extracellular signal-regulated kinase 1 (ERK1) protects leptin-deficient mice from insulin resistance without affecting obesity. Diabetologia 2011;54:180-189
22. Mari M, Monzo P, Kaddai V, Gonzalez T, Le Marchand-Brustel Y, Cormont M. The Rab4 effector Rabip4 plays a role in intracellular trafficking of Glut 4 in 3T3-L1 adipocytes. J Cell Sci 2006;119:1297-1306
23. Gilleron J, Querbes W, Zeigerer A, Borodovsky A, Marsico G, Schubert U, Manygoats K, Seifer S, Andree C, Stöter M, Epstein-Barash H, Zhang L, Koteliansky V, Fitzgerald K, Fava E, Bickle M, Kalaidzidis Y, Akinc A, Maier M, Zerial M. Image-based analysis of lipid nanoparticle-mediated siRNA delivery, intracellular trafficking and endosomal escape. Nat Biotechnol 2013;31:638-646
24. Renier N, Wu Z, Simon DJ, Yang J, Ariel P, Tessier-Lavigne M. iDISCO: a simple, rapid method to immunolabel large tissue samples for volume imaging. Cell 2014;159:896-910
25. Ritchie ME, Phipson B, Wu D, Hu Y, Law CW, Shi W, Smyth GK. limma powers differential expression analyses for RNA-sequencing and microarray studies. Nucleic Acids Res 2015;43:e47
26. Kaddai V, Gonzalez T, Bolla M, Le Marchand-Brustel Y, Cormont M. The nitric oxide-donating derivative of acetylsalicylic acid, NCX 4016, stimulates glucose transport and glucose transporters translocation in 3T3-L1 adipocytes. Am J Physiol Endocrinol Metab 2008;192:E162-E169
27. Dizdaroglu M, Jaruga P. Mechanisms of free radical-induced damage to DNA. Free Radic Res 2012;46:382-419
28. Munoz-Espin D, Serrano M. Cellular senescence: from physiology to pathology. Nat Rev Mol Cell Biol 2014;15:482-496
29. Hock AK, Vousden KH. The role of ubiquitin modification in the regulation of p53. Biochem Biophys Acta 2014;1843:137-149
30. Arner P, Langin D. Lipolysis in lipid turnoveer, cancer cachexia, and obesity-induced insulin resistance. Trends Endocrinol Metab 2014;25:255-262
31. Brasaemle DL. Thematic review series: adipocyte biology. The perilipin family of structural lipid droplet proteins: stabilization of lipid droplets and control of lipolysis. J Lipid Res 2007;48:2547-2559
32. Tanaka N, Takahashi S, Matsubara T, Jiang C, Sakamoto W, Chanturiya T, Teng R, Gavrilova O, Gonzalez FJ. Adipocyte-specific disruption of fat-specific protein 27 causes hepatosteatosis and insulin resistance in high-fat diet-fed mice. J Biol Chem 2015;290:3092-3105
33. Ortega FJ, Moreno-Navarrete JM, Mayas D, Serino M, Rodriguez-Hermosa JI, Ricart W, Luche E, Burcelin R, Tinahones FJ, Frûhbeck G, Mingrone G, Fernandez-Real JM. Inflammation and insulin resistance exert dual effects on adipose tissue tumor protein 53 expression. Int J Obes 2014;38:735-745
34. Yokoyama M, Okada S, Nakagomi A, Moriya J, Shimizu I, Nojima A, Yoshida Y, Ichimiya H, Kamimura N, Kobayashi Y, Ohta S, Fruttiger M, Lozano G, Minamino T. Inhibition of endothelial p53 improves metabolic abnormalities related to dietary obesity. Cell Rep 2014;7:1691-1703
35. Inoue N, Yahagi N, Yamamoto T, Ishikawa M, Watanabe K, Matsuzaka T, Nakagawa Y, Takeuchi Y, Kobayashi K, Takahashi A, Suzuki H, Hastry AH, Toyoshima H, Yamada N, Shimano H. Cyclin-dependent kinase inhibitor, p21 WAF1/CIP1, is involved in adipocyte differentiation and hypertrophy, linking to obesity, and insulin resistance. J Biol Chem 2008;283:21220-21229
36. Cooke MS, Evans MD, Dizdaroglu M, Lunec J. Oxidative DNA damage: mechanisms, mutation, and disease. Faseb J 2003;17:1195-1214
37. Eriksson JW. Metabolic stress in insulin's target cells leads to ROS accumulation - a hypothetical common pathway causing insulin resistance. FEBS Lett 2007;581:3734-3742
38. Vieira-Potter VJ. Inflammation and macrophage modulation in adipose tissues. Cell Microbiol 2014;16:1484-1492
39. Chatzinikolaou G, Karakasilioti I, Garinis GA. DNA damage and innate immunity: links and trade-offs. Trends Immunol 2014;35:429-435
40. Surmi BK, Hasty AH. The role of chemokines in recruitment of immune cells to the artery wall and adipose tissue. Vascul Pharmacol 2009;52:27-36

41. Huh JY, Park YJ, Ham M, Kim JB. Crosstalk between adipocytes and immune cells in adipose tissue inflammation and metabolic dysregulation in obesity. Mol Cells 2014;37:365-371
42. Ceppo F, Berthou F, Jager J, Dumas K, Cormont M, Tanti J-F. Implication of the Tpl2 kinase in inflammatory changes and insulin resistance induced by the interaction between adipocytes and macrophages. Endocrinology 2014;155:951-964
43. Shimizu I, Yoshida Y, Moriya J, Nojima A, Uemura A, Kobayashi Y, Minamino T. Semaphorin3E-induced inflammation contributes to insulin resistance in dietary obesity. Cell Metab 2013;18:491-504
44. Girousse A, Tavernier G, Valle C, Moro C, Mejhert N, Dinel AL, Houssier M, Roussel B, Besse-Patin A, Combes M, Mir L, Monbrun L, Bézaire V, Prunet-Marcassus B, Waget A, Vila I, Caspar-Bauguil S, Louche K, Marques MA, Mairal A, Renoud ML, Galitzky J, Holm C, Mouisel E, Thalamas C, Viguerie N, Sulpice T, Burcelin R, Arner P, Langin D. Partial inhibition of adipose tissue lipolysis improves glucose metabolism and insulin sensitivity without alteration of fat mass. PLoS Biol 2013;11:e1001485
45. Herman MA, Peroni OD, Villoria J, Schön MR, Abumrad NA, Blüher M, Kleins S, Kahn BB. A novel ChREBP isoform in adipose tissue regulates systemic glucose metabolism. Nature 2012;484:333-338
46. Roberts R, Hodson L, Dennis AL, Neville MJ. Markers of de novo lipogenesis in adipose tissue: associations with small adipocytes and insulin sensitivity in humans. Diabetologia 2009;52:882-890

Figure legends

Figure 1. Adipocytes of obese mice exhibit activation of the p53 pathway with an increase in DNA damage and a reduction in telomere length.

Level of p21 mRNA in epididymal adipose tissue (AT) and isolated adipocytes (Ad) of *ob/ob* (*A*) and HFD mice (18 weeks of 60% kcal from fat) (*B*) and their lean control littermates (n=8 per group). p21 mRNA expression was normalized using mouse Rplp0 mRNA level and expressed in arbitrary units with the control value (*ob*/+ or normal chow diet NCD mice) taken as 1. *C*: Western blot analysis of the expression p53 (anti-p53 #2524, Cell Signaling) and p21 (anti-p21, clone CP74, P1484, Sigma-Aldrich) in isolated adipocytes from HFD and NCD fed mice with tubulin (anti-tubulin T6199, Sigma-Aldrich) as loading control. Each lane corresponds to independent preparations of adipocytes. *D*: Immunofluorescence analysis of p21 in nucleus of isolated adipocytes from HFD and NCD mice. DAPI was used to visualize the nuclei. Representative images and quantification of nuclei with detectable p21 labeling in 15-20 cells per adipocyte preparation (n=8) were shown. *E*: Amounts of 8-OHdG quantified in total DNA from AT of mice fed a NCD or a HFD (45% or 60% of kcalories from fat, n=8 per group). Results are expressed in pg of oxidized dG per µg of AT DNA. *F*: Correlation between amounts of AT oxidized DNA and AT p21 mRNA expression. Red dots: NCD-fed mice, blue dots: 45 % HFD fed mice, black dots: 60% HFD fed mice. *G*: Relative telomere length was estimated from total DNA prepared from AT of NCD and HFD mice (n=8 per group). Results are expressed in arbitrary units with the NCD mice taken as 1. *H and I*: Isolated adipocytes from NCD and HFD mice (60 % kcal from fat) were treated for immunofluorescence as in (*D*). Immunodetection was performed with anti γH2AX (Ser139) antibodies (Millipore 05-636) followed by anti-mouse antibodies coupled to AlexaFluor488. Nuclei were labeled by DAPI. The quantifications of the foci number were performed on 10-

15 cells per adipocytes preparations (n=8 per group) and the graph represents the number of cells as a function of the foci number.

Data are means ± SEM with * $p < 0.05$, ** $p < 0.01$, *** $p < 0.001$.

Figure 2. DNA damage in the adipocyte is an early event during obesity development.

A: representative images of cleared adipose tissues from NCD-fed and HFD-fed mice (HFD feeding for 2 or 4 weeks) labeled with γ-H2AX antibodies (green), DAPI (blue), phalloïdin (red) together with enlarged views of the delineated regions. Images were acquired with a NikonA1 confocal with a 20x long-working-distance objective, allowing for acquisitions up to 3 mm into the tissue. A mosaic of 9 images over 1 mm was randomly acquired and blindly quantified. Z-projections along the z-axis were generated and the DAPI (blue) and phalloidin (red) images were merged to discriminate nuclei from small cells that were entirely surrounded by F-actin (purple nuclei) from nuclei of mature adipocytes that were not surrounded by F-actin (blue nuclei). Adipocyte nuclei without DNA damage are blue (only DAPI labeling, arrows). They are cyan when DNA damage was present (merge of DAPI-blue and γ-H2AX -green, arrow heads). Nuclei from other smaller cells without DNA damage are purple (merge of DAPI-blue and phalloïdin-red) and are white with DNA damage (merge of DAPI-blue, γ-H2AX antibodies-green, and phalloïdin-red). *B:* Quantification of the number of adipocytes presenting DNA damage in their nucleus using the colocalization pluging of FiJi. Data are expressed as the % of cells with DNA damage and are means ± SEM with ** $p < 0.01$, *** $p < 0.001$ HFD versus NCD mice and $^{###}p < 0.001$ HFD 4 weeks versus HFD 2 weeks. *C:* Left panel, quantification of ROS using DHE labeling on AT sections from mice fed a NCD or a HFD for 2 weeks and 4 weeks; Right panel, quantification of ROS production by isolated adipocytes from mice fed a NCD or a HFD for 2 weeks using the ROS probe H2DCFDA. Data are means ± SEM with *$p < 0.05$, **$p < 0.01$, ***$p < 0.001$ versus NCD mice. *D:* Western blot analysis of the expression of p53 (n=3 representative mice per group)

and quantification of p53 protein expression in AT after NCD or HFD feeding for 2 weeks (n=13 per group) or 4 weeks (n=5 for NCD and 6 for HFD). Right panel: quantification of the indicated mRNA in AT after NCD or HFD feeding for 2 weeks (n=7 mice per group). Results are expressed relative to the NCD-fed mice. Data are means ± SEM with * $p < 0.05$, ** $p < 0.01$, *** $p < 0.001$. *E*: Insulin effect on lipogenesis in isolated adipocytes from mice fed a NCD or HFD for 2 weeks (n=6 adipocyte preparations from 6 different mice in each of the groups). Data are expressed as fold increase over unstimulated cells. *F*: quantification of the mRNA levels of the indicated genes in AT from mice fed a NCD or HFD during 2 weeks (n=7 mice per group). Data are means ± SEM with ** $p < 0.01$. ***G***: IPGTT in mice fed a NCD or HFD during 2 weeks. Area under the curve (AUC) was calculated from 0 to 120 min. *H*: HOMA-IR index (fasting glucose mM x fasting insulin µU/ml/22.5) of the same mice as in *G*. *I*: Left panel, quantification by flow cytometry analysis of the numbers of $F4/80^+$ ($CD11c^+$ or $CD11c^-$) and $F4/80^-CD11c^+$ cells in the SVF from mice fed a NCD or a HFD during 2 weeks (n=6 mice per group). Values represent the number ± SEM of each of the cell subtypes per gram of epididymal fat tissues. Fluorescent-coupled anti F4/80 and CD11c were from eBioscience. Middle panel, quantification of the mRNA expression of markers of inflammation in AT of the same mice. Right panel, concentration of IL-6 and TNF-α in sera of mice fed a NCD or HFD for 2 or 18 weeks (as a positive control). Data are means ± SEM with * $p < 0.05$, ** $p < 0.01$, ***$p < 0.01$ HFD versus NCD 2 weeks and $^{\#}p < 0.05$, $^{\#\#}p < 0.01$ HFD 18 weeks versus NCD 18 weeks.

Figure 3. ***In vivo*** **doxorubicin treatment induces AT inflammation and adipocyte insulin resistance.**

Mice were injected with doxorubicin (doxo) or vehicle (ctrl, n=6 per group) for 42 h before analysis of the adipose tissue (AT), the adipocytes (Ad), and the stroma vascular fraction (SVF). *A*: Quantification by flow cytometry analysis of the number of $F4/80^+$ ($CD11c^+$ or

$CD11c^-$) and $F4/80^-CD11c^+$ cells in the SVF from control or doxorubicin-treated mice. Values represent the number ± SEM of each of the cell subtypes per gram of epididymal fat tissues. *B*: Frozen sections of AT were subjected to Hematoxylin/Eosin (H/E) coloration (top) and to immunodetection (bottom) with a FITC-coupled anti-Lys6G antibody (Biolegends) and nuclei were labeled using DAPI. A representative image from a control and a doxorubicin-treated mouse was shown. For quantification, 5 images/mouse were automatically captured and the percentage of cells positive for Lys6G was determined. *C*: Western blot analysis of the level of phospho-p65-NFκB (anti-p-p65 NFκB #3033, Cell Signaling) in the SVF from control or doxorubicin-treated mice with Rho-GDI as loading control (anti Rho-GDI A20 sc-360, Santa Cruz). Each lane corresponds to independent mice. *D-E*: Relative expression of the indicated mRNAs in AT, adipocytes (Ad), and the stroma vascular fraction (SVF) from control and doxorubicin-treated mice mice. The mRNA expression was normalized using mouse Rplp0 mRNA level and expressed in arbitrary units with the control mice taken as 1. AdipoQ is for adiponectin. *F*: Left panel, insulin effect on lipogenesis in isolated adipocytes from control or doxorubicin-treated mice (n=4 adipocyte preparations from 4 different mice in each of the groups). Data are expressed as fold over unstimulated cells. Right panel, western blot analysis of the expression of p-PKB (anti-pPKB Ser473 #4058, Cell Signaling), PKB (anti-PKB #9272, Cell Signaling), and Glut4 (anti-Glut4 1F8 sc-53566, Santa Cruz) in isolated adipocytes from control and doxorubicin-treated mice with Rho-GDI as loading control. *G*: quantification of Free Fatty Acids (FFA) in sera from control and doxorubicin-treated mice (NEFA FS kit, DiaSys). *H*: IPGTT in control and doxorubicin-treated mice. Area under the curve (AUC) was calculated from 0 to 120 min. *I*: Quantification of insulinemia in sera of mice before the injection of glucose and 20 min after glucose injection during the IPGTT shown in *H*. Data are means ± SEM with * p <0.05, ** p < 0.01, ***p <0.001 versus control mice.

Figure 4. Impact of adipocytes-p53 activation on macrophage activation and macrophage and neutrophil migration.

A, B, D: 3T3-L1 adipocytes were treated for 48 h with 10 µM nutlin-3 (Enzo Life Sciences) or 24 h with 0.5 µg/ml doxorubicin (doxo). Then cells were thoroughly rinsed and fresh medium was added and the conditioned media (AdCM) were collected for the following 24 h. *A*: RAW-blue^{TM} macrophages were incubated with conditioned media (AdCM) or control culture medium (M) for 24 h and the activity of the alkaline phosphatase released in the media was quantified as readout of RAW-blue^{TM} activation. LPS (0.5 ng/ml) was added in control medium or AdCM as a positive control for macrophage activation. Quantification of 3 independent experiments normalized to cells treated with control medium is shown and expressed as means ± SEM. *B*: Chemotaxis assay was performed with RAW264.7 macrophages using the indicated conditioned media (AdCM) or control media (M). The number of macrophages stained by crystal violet having performed chemotaxis was counted by analyzing 10 fields for each experimental condition. A typical field corresponding to each of the experimental condition was shown. Results were normalized relative to the number of macrophages attracted by control medium (M). Data are means ± SEM of 3 independent experiments with ** $p < 0.01$ control medium versus control AdCM (AdCM from untreated adipocytes). $^{\#}$ $p < 0.05$, $^{\#\#\#}$ $p < 0.001$ AdCM from adipocytes treated with drugs versus control AdCM. *C*: Human cultured adipocytes were treated for 48 h with 10 µM nutlin-3 or 24 h with 0.75 µg/ml doxorubicin (doxo). Conditioned media (AdCM) were collected as described above. Chemotaxis assay was performed with blood monocyte-derived macrophages using the indicated AdCM. Results were normalized relative to the number of macrophages attracted by control AdCM. Data are means ± SEM of 3 experiments with 3 AdCM collected from 3 independent cultures of human adipocytes with the same human monocyte-derived macrophage preparation. * $p < 0.05$ versus control AdCM. *D*: The number of neutrophils

having performed chemotaxis towards media (M), fMLP (0.2 μM a chemotactic factor for neutrophils), AdCM of control, nutlin, or doxorubicin-treated adipocytes was determined by quantifying the number of $CD11b^{+}Lys6G^{+}$ cells in the lower Boyden chamber by flow cytometry analysis. Top, representative flow cytometry plots for $CD11b^{+}Lys6G^{+}$ cells that have migrated towards AdCM from control, nutlin, or doxorubicin-treated cells. Bottom, quantification of the number of migrating neutrophils in chemotaxis assays performed with 4 independent AdCM and one white blood cell preparation. The experiment was reproduced twice. $*p < 0.05$, $**p < 0.01$, $***p < 0.001$ versus control AdCM.

Figure 5. Effect of DNA damage and p53 activation on cytokines/chemokines mRNA expression and the implication of p53.

A: 3T3-L1 adipocytes were treated with 0.5 μg/ml doxorubicin (doxo) for 24 h or 10 μM nutlin-3 (nutl) for 48 h. Total RNA were then prepared and used in gene expression profiling by microarray. The figure represents the changes in the level of expression of cytokines and chemokines between doxorubicin-treated *vs* control adipocytes as a function of the changes in the level of expression between nutlin-treated *vs* control adipocytes. Changes are expressed in Log_2. Only the cytokines/chemokines that have an expression changed in one or the two experimental conditions were shown. *B and C*: Relative mRNA amount of the indicated chemokines/cytokines in 3T3-L1 adipocytes transfected with control siRNA (si ctrl) or p53 siRNA (si p53) and incubated without (ctrl) or with nutlin-3 (*B*) or doxorubicin (*C*). When indicated, adipocytes transfected with p53 siRNA were also treated with pifithrin-α (pif). Data (n=3-4 independent experiments) are normalized using mouse Rplp0 mRNA level and expressed as arbitrary units with the value of si ctrl untreated cells taken as 1 (dashed line in *C*). *D*: Relative mRNA expression of the indicated chemokines in adipose tissue (AT), adipocyte (Ad), and stromal vascular fraction (SVF) of control mice or doxorubicin-treated mice. The measurements were performed with the same mRNA samples than those used in

Fig. 3*D, E. E-F:* Relative mRNA expression of the indicated chemokines in adipose tissue (AT) of mice fed a normal chow diet (NCD) or high fat diet (HFD) for 2 weeks (*E*) or *4* weeks (*F*). The measurements were performed with the same mRNA samples as in Fig 2*F-I* and supplementary Fig *E*, *F*.

Data are means ± SEM with * p <0.05, ** p < 0.01, *** p <0.001 versus effect in untreated si ctrl cells or in mice injected with vehicle, or in NCD-fed mice, $^{\#}p$ < 0.05, $^{\#\#}p$ < 0.01 drug-treated si ctrl cells versus drug-treated si p53 cells.

Figure 6. **Inhibition of insulin-induced glucose transport and Glut4 translocation in adipocytes treated with doxorubicin or nutlin-3.**

3T3-L1 adipocytes were treated with 0.5 µg/ml doxorubicin (doxo) for 24 h or 10 µM nutlin-3 (nutlin) for 48 h and stimulated with the indicated concentrations of insulin for 10 min. *A and B*: Measurement of deoxyglucose (DOG) uptake (n=3 independent experiments). *C, D*: Representative Western blot analysis and quantification (n= 4 independent experiments) of the protein expression of the glucose transporters Glut4 (anti-Glut4 1F8, Santa Cruz) and Glut1 (anti Glut1 ab652, Abcam) with tubulin as loading control. *E, F*: Glut4 translocation was determined by the quantification of Glut4 amount in plasma membrane lawns. Quantification of 26 fields obtained in two independent experiments (top panels) and representative fields (bottom panels) were shown.

Data are means ± SEM with * p <0.05, * p <0.01, *** p <0.001 untreated cells stimulated with insulin versus drug-treated cells stimulated with insulin.

Figure 7. **Inhibition of insulin signaling in 3T3-L1 adipocytes treated with doxorubicin or nutlin-3**.

3T3-L1 adipocytes were treated with 0.5 µg/ml doxorubicin for 24 h (doxo) or 10 µM nutlin-3 (nutlin) for 48 h and incubated without or with insulin (ins, 0.5 nM) for 10 min. *A and B*: Representative western blot analysis and quantification (n= 3-4 independent experiments) of

the expression of the tyrosine phosphorylated (anti-PhosphoTyrosine #9411, Cell Signaling) insulin receptor (pY-IR) and IRS (pY-IRS), the pThr308-PKB (p-PKB, anti-pThr308-PKB #4056, Cell Signaling), total PKB and p53. Data are expressed as percentage of insulin effect in untreated cells stimulated with insulin. Normalization was performed by quantifying ERK (anti-ERK1/2 #4695, Cell Signaling) or HSP90 (anti-HSP90 sc-13119, Santa Cruz) in each of the experiments. *C*: 3T3-L1 adipocytes were treated for 24 h with 0.5 µg/ml doxorubicin (doxo) or for 48h with nutlin-3 (10 µM) and the conditioned media (AdCM) was collected as described in figure 4. 3T3-L1 adipocytes were incubated with AdCM for 24 h, washed and incubated without or with insulin (ins, 0.5 nM) for 10 min, before lysis for western blot analysis of PKB phosphorylation. Representative immunoblot and quantification of 3 independent experiments are shown. The ratios of PThr308-PKB (p-PKB) relative to HSP90 are expressed as percentage of insulin effect in cells treated with control AdCM. *D and E:* 3T3-L1 adipocytes were transfected with control siRNA (si Ctrl) or p53 siRNA (si p53). The cells treated with p53 siRNA were also incubated with pifithrin-α (pif, 50 µM). Cells were incubated with 0.5 µg/ml doxorubicin for 24 h (*D*) or with 10 µM nutlin-3 for 48 h (*E*). Adipocytes were then stimulated with 0.5 nM insulin for 10 min. Western blot analysis of p53 and p21 expression (left panels) and pThr308-PKB (p-PKB) and total PKB expression (right panels) with HSP90 as loading control. Representative immunoblots are shown and quantifications are presented in the supplemental figure 5.

Data are means $\pm$ SEM with * $p < 0.05$, ** $p < 0.01$, *** $p < 0.001$ untreated cells stimulated with insulin versus drug-treated cells stimulated with insulin

Figure 8. Doxorubicin and nutlin-3 stimulate lipolysis in adipocytes.

A-B: Glycerol release was measured as an index of lipolysis, in the medium of 3T3-L1 adipocytes transfected with control siRNA (si ctrl) or p53 siRNA (si p53) and treated with nutlin-3 (*A*) or doxorubicin with or without pifithrin-α (pif) (*B*). Data are expressed as fold

increase over control cells (untreated cells transfected with si ctrl) and are presented as means ± SEM of 3-4 independent experiments with *** $p < 0.001$ untreated si ctrl cells *vs* drug-treated si ctrl cells, $^{\#}p < 0.05$, $^{\#\#}p < 0.01$ drug-treated si ctrl cells *vs* drug-treated si p53 cells. *C*: 3T3-L1 adipocytes were treated with 0.5 µg/ml doxorubicin (doxo) for 24 h or 10 µM nutlin-3 (nutl) for 48 h. Total RNA were then prepared and used in gene expression profiling. The figure represents the changes in the level of expression of genes involved in lipolysis between doxorubicin-treated *vs* control adipocytes as a function of the changes in the level of expression between nutlin-treated *vs* control adipocytes. Changes are expressed in Log_2. The name of genes down-regulated in both doxorubicin and nutlin-treated adipocyte were indicated. *D*: Representative western blot and quantification (n= 3 independent experiments) of the expression of perilipin 1 (*PLN1* gene) using an anti-perilipin 1 antibody (D418, Cell Signaling) with HSP90 as loading control. Data are means ± SEM with *$p < 0.05$ nutlin- or doxorubicin-treated cells versus control

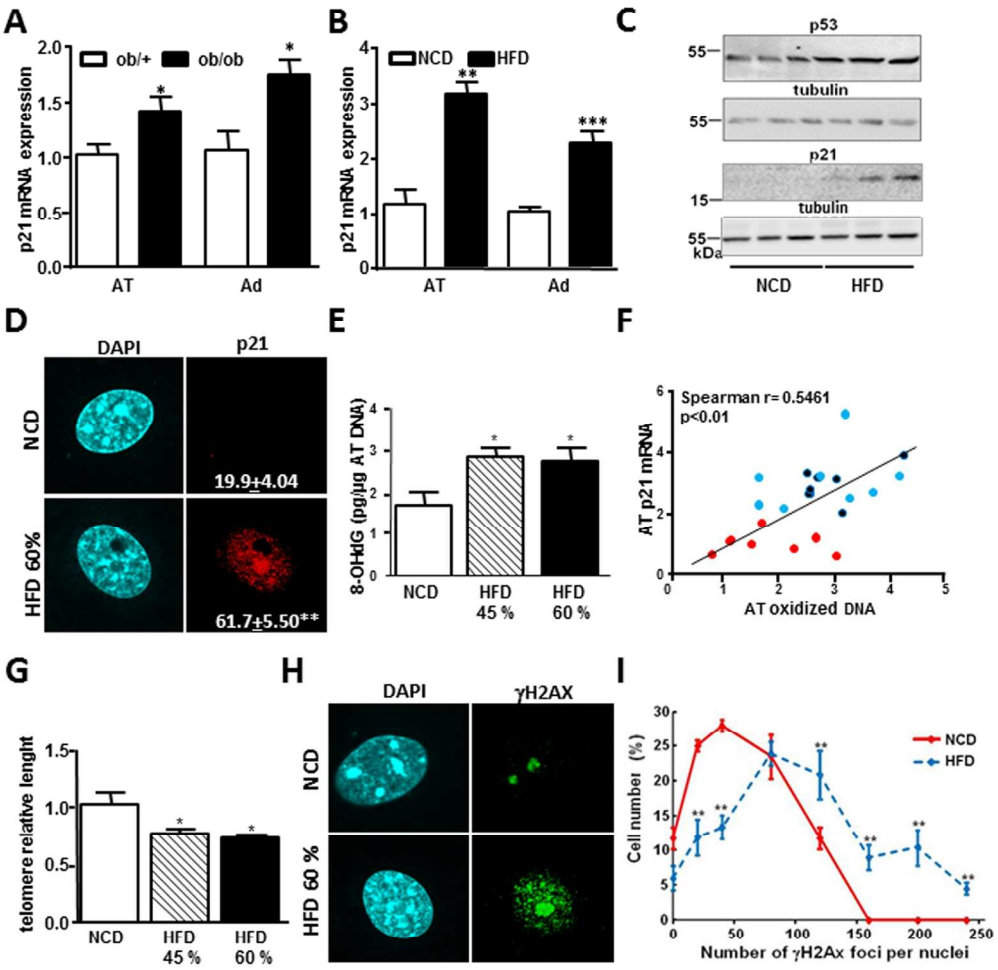

Figure 1

180x204mm (300 x 300 DPI)

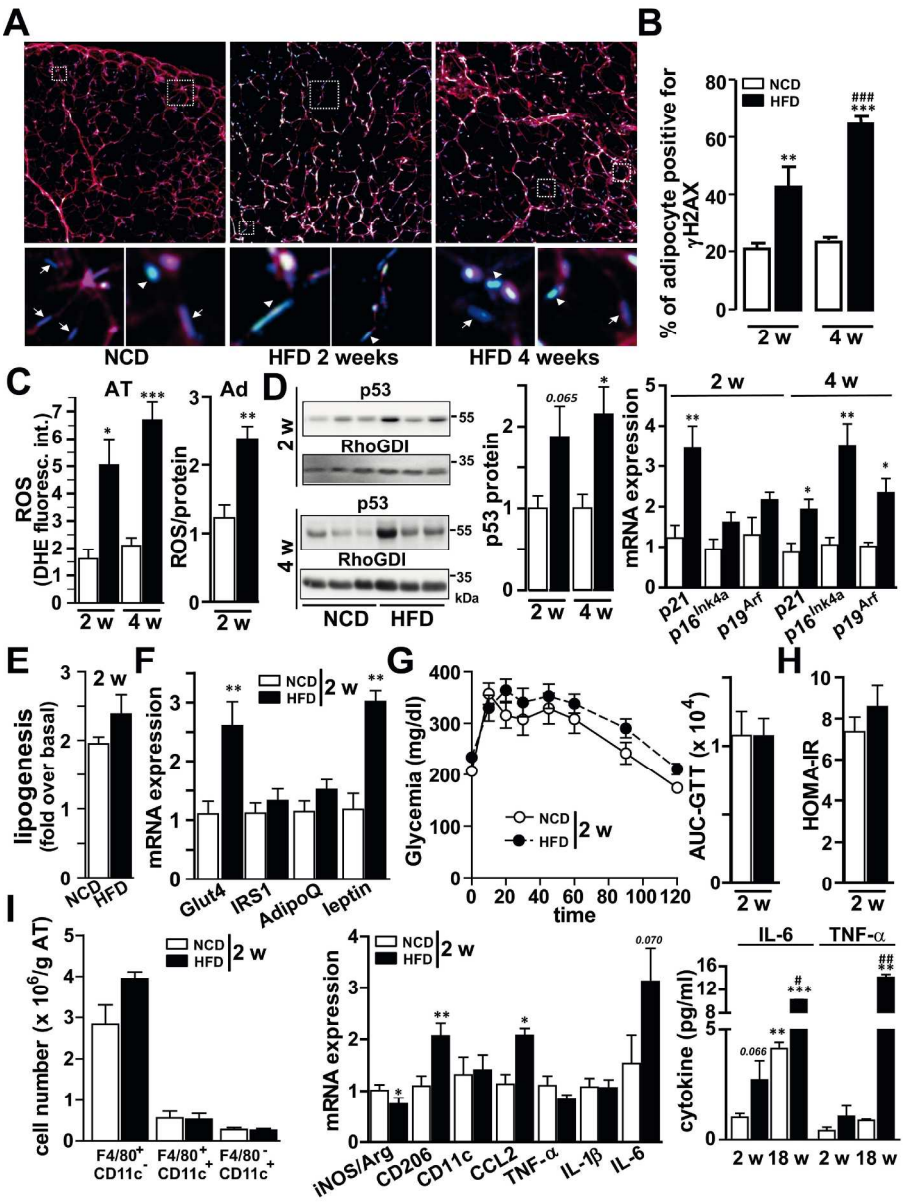

Figure 2

213x285mm (300 x 300 DPI)

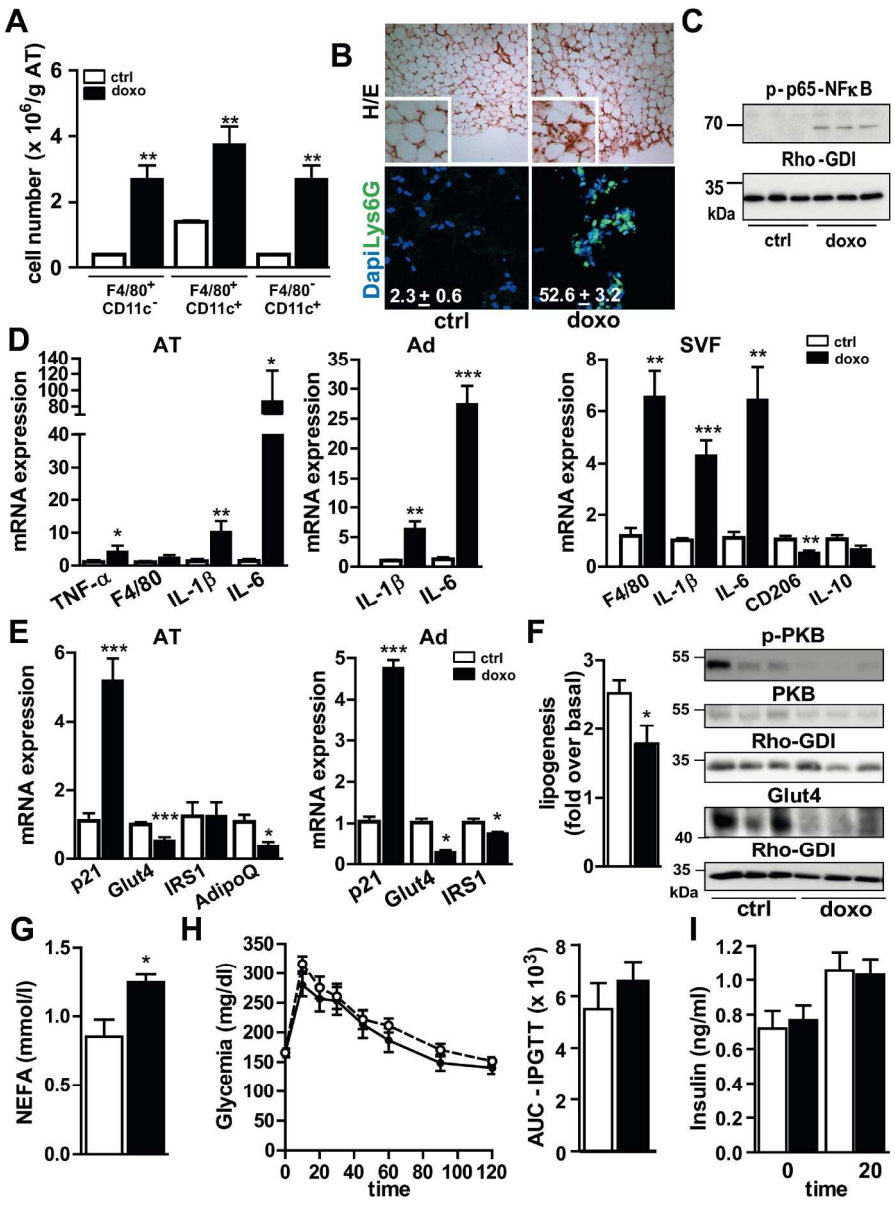

Figure 3

215x290mm (300 x 300 DPI)

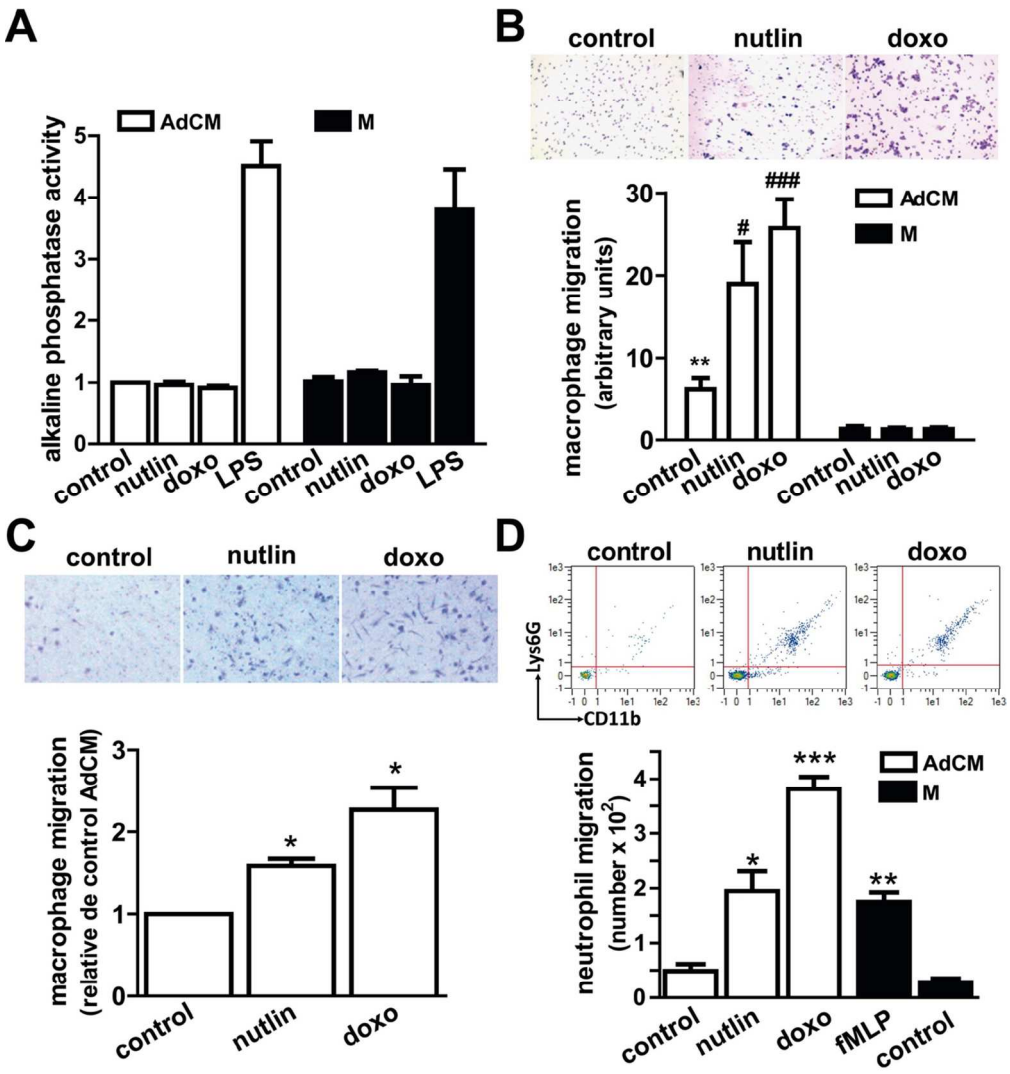

Figure 4

128x138mm (300 x 300 DPI)

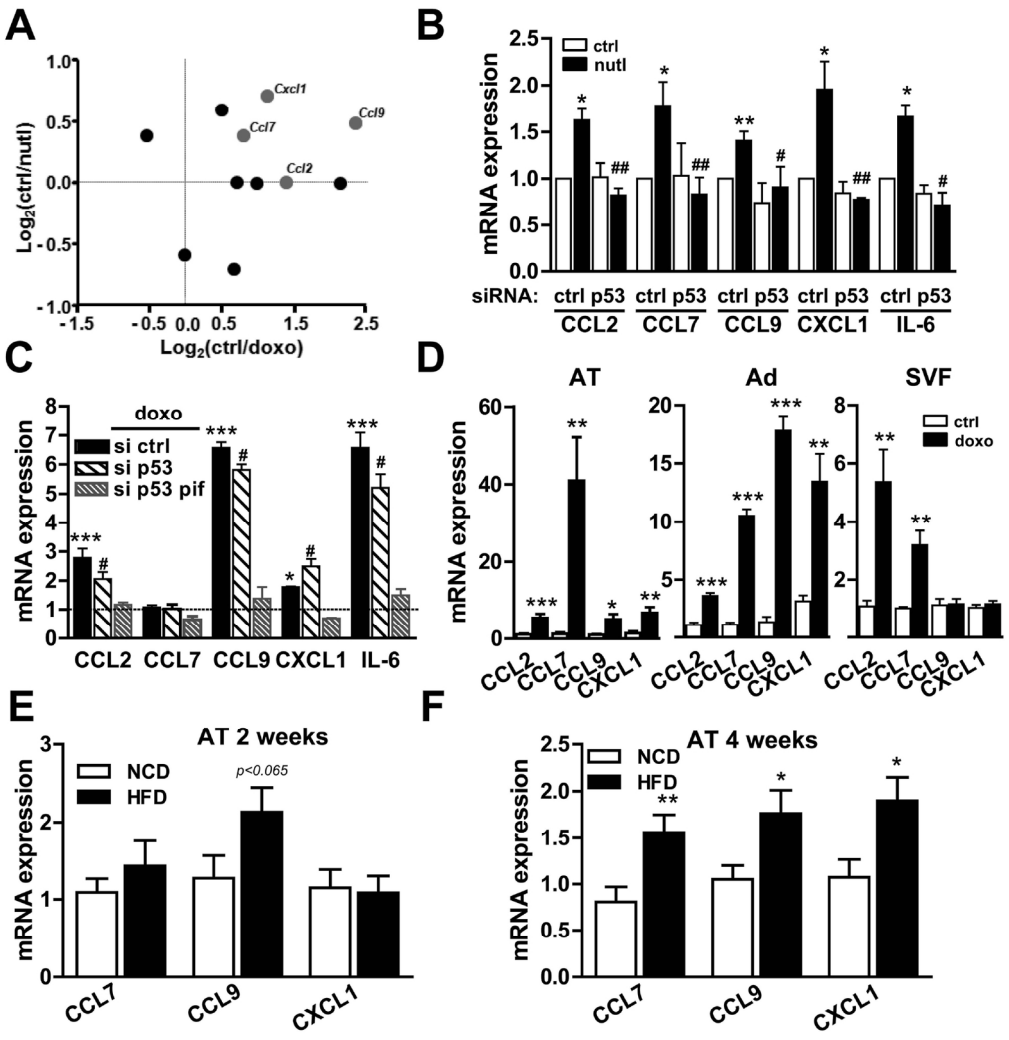

Figure 5

165x171mm (300 x 300 DPI)

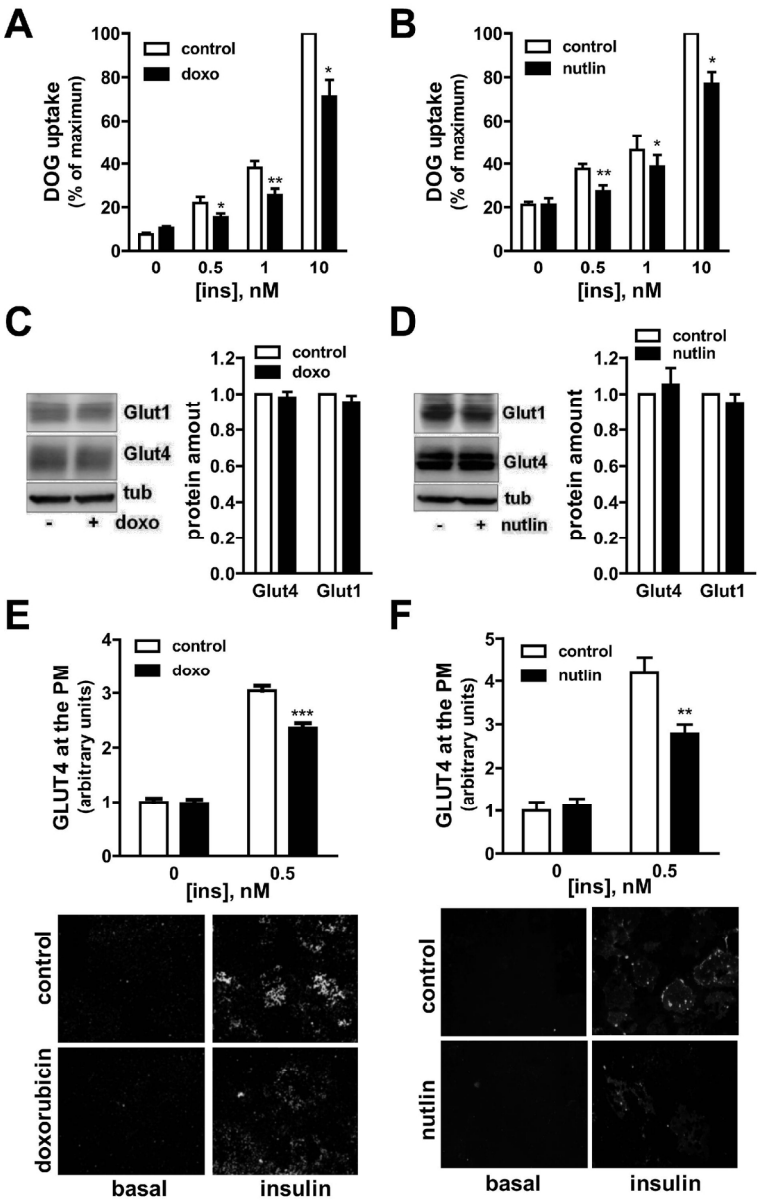

Figure 6

127x203mm (300 x 300 DPI)

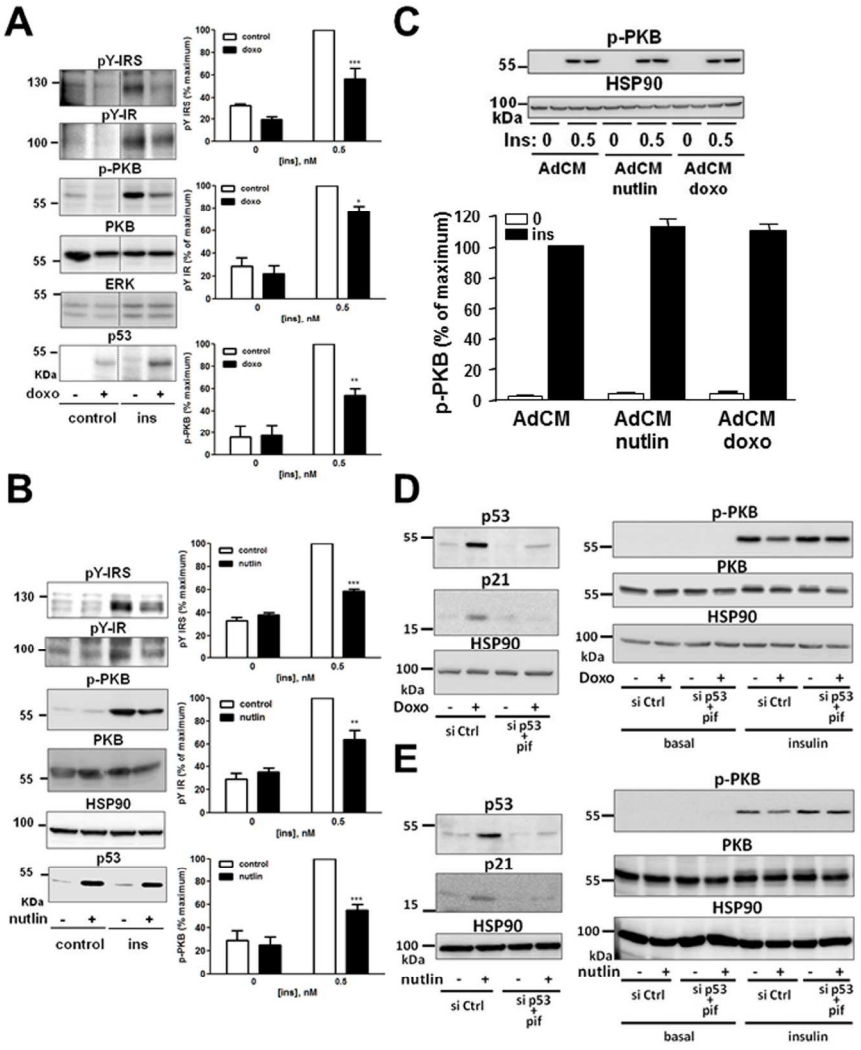

Figure 7

213x284mm (300 x 300 DPI)

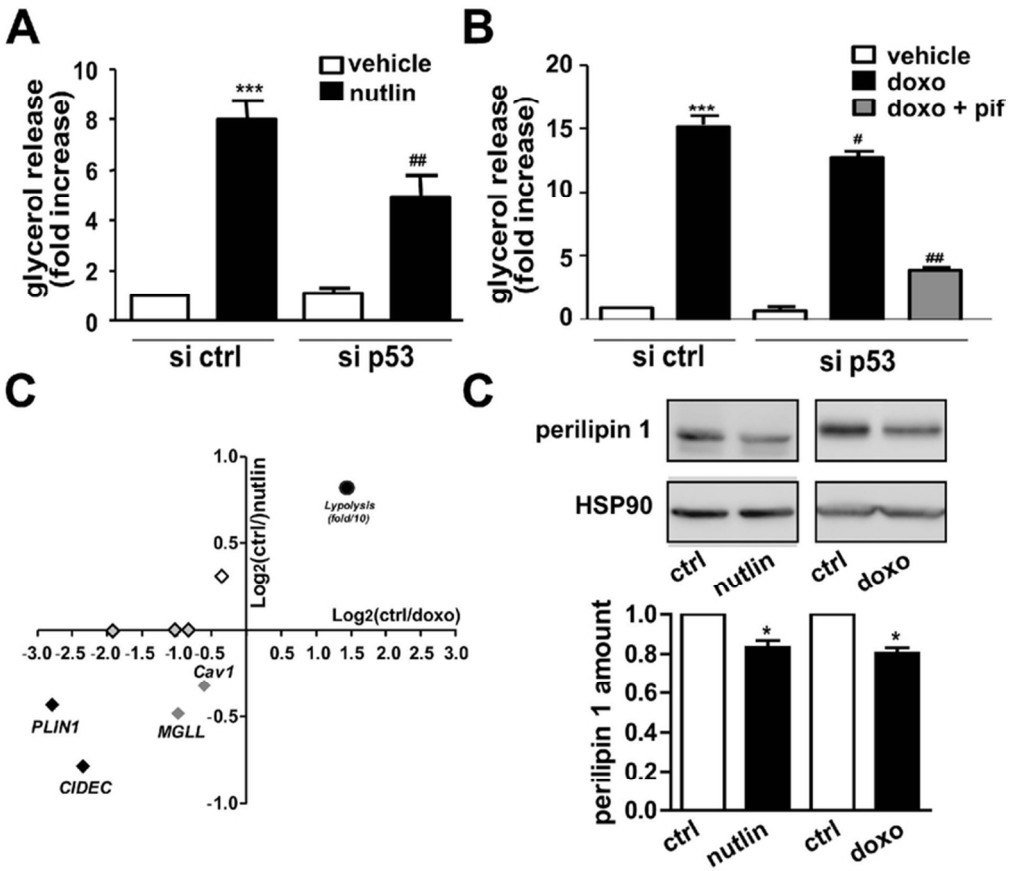

Figure 8

69x60mm (300 x 300 DPI)

Online Supplemental Table 1

Characteristics of the normal-chow fed mice and the high-fat fed mice.

	Body Weight (g)	Fat pads Weight (mg)	Fasting Glycemia (mg/dl)	IPGTT AUC (arbitrary unit)
Normal chow (n=32)	28.76 ± 0.35	605 ± 83.25	165.3 ± 7. 86	7121 ± 1466
high-fat 45 % (n=8)	37.80 ± 0.90 ***	2330 ± 151.1***	205.5 ± 11.97*	13734 ± 1527**
high-fat 65 % (n=16)	44.31 ± 1.54*** ###	2817 ± 180.4***	246.0 ± 7.11*** #	18540 ± 1171***

Data are means ± SEM. Comparison between groups was performed with ANOVA and Bonferroni post-hoc test in the case of 18 week-diet. * P< 0.05, ** P< 0.01, *** P< 0.001 standard chow *vs* high-fat diet; # P<0.05, high-fat diet 65 % *vs* high-fat diet 45 %.

Online Supplemental Table 2

Correlative analysis between telomere length, p21 mRNA expression, obesity, and glycemia

	Body weight	Fat pads weight	Fasting glycemia	p21 mRNA level
Telomere length	-0.549 **	-0.573 **	-0.533**	-0.430*
p21 mRNA level	0.720 ***	0.684 ***	0.494 *	

Telomere length and p21 mRNA level were measured in adipose tissue from mice fed a normal chow-diet (n=8) or a high-fat diet (45 % and 60 % kcal from fat, n=8 for each diet) and correlated to each other and to body weight, fat pads weight and fasting glycemia by Spearman correlation test. Spearman r was indicated in the table. * $P< 0.05$, ** $P< 0.01$ and *** $P< 0.001$.

Supplemental figure legends

Supplemental Figure 1. Characterization of mice fed a high-fat diet for 2 or 4 weeks vs mice fed a normal chow diet.

A: Weight of the epididymal adipose tissue (epiAT). *B*: Mean adipocyte diameter (left) and adipocyte number distribution relative to their diameter (right). *C:* Serum glucose and insulin levels in 6 h-fasted mice fed a NCD or a HFD for 2 weeks (n =13 mice per groups analyzed in two independent experiments) *D:* Serum glucose and insulin level in the same mice as in *C* but random fed. *E:* IPGTT in mice fed a NCD (n=5) or HFD (n=6) for 4 weeks. *F*: Serum glucose and insulin levels in 6 h-fasted mice fed a NCD (n=5) or a HFD (n=6) for 4 weeks. *G*: Serum glucose and insulin level in the same mice as in *F* but random fed. *H*: Body weight gain of the mice after 2 or 4 weeks of HFD. *I-J*: Expression of the mRNA expression of the indicated genes in AT of mice fed a NCD or HFD for 4 weeks. *K*: Quantification of neutrophil infiltration in AT of mice fed a NCD or HFD for 2, 4, and 18 weeks by immunodetection on AT section with anti-Lys6G antibodies as described in Figure 3. *L*: Quantification of immune cells by flow cytometry in the SVF of AT from mice fed a NCD or HFD for 2 weeks. The CD11b and Lys6G were used to quantify neutrophils, CD3 for T lymphocytes, and B220 for B lymphocytes. Results are expressed as the number of cells per g of epididymal AT.

Date are means + SEM with * $p < 0.05$, ** $p < 0.01$ and *** $p < 0.001$ versus NCD-fed mice

Supplemental Figure 2. Induction of DNA damage by doxorubicin and nutlin-3 and effect of p53 siRNA on p53 and p21 expression

3T3-L1 adipocytes cultured on glass coverslips were treated for 24 h with 0.5 µg/ml of doxorubicin or for 48 h with 10 µM nutlin-3. Adipocytes were then treated for immunofluorescence for γ-H2AX labeling (*A*) or p21 labeling (*B*) and nucleus detection by

using DAPI. The bar corresponds to 10 μm. The arrow heads point to p21-labeled nuclei. *C*: Western blot analysis of the expression of the indicated protein in 3T3-L1 adipocytes transfected with control siRNA (ctrl) or p53 siRNA and then treated with 10 μM nutlin-3 (nutlin) or with 0.5 μM of doxorubicin. Hsp90 as loading control. A representative experiment was shown.

Supplemental Figure 3. Conditioned media from doxorubicin or nutlin-3-treated adipocytes do not modify macrophages polarization

A: 3T3-L1 adipocytes were treated for 48 h with 10 μM nutlin-3 (nutlin), 24 h with 0.5 μg/ml doxorubicin (doxo), or vehicle (control). Cells were then thoroughly rinsed and fresh medium was added and the conditioned media was collected for the following 24 h. RAW-blue™ macrophages were incubated with the conditioned media for 24 h and the RNA were extracted in order to quantify the expression of the indicated markers for M1-type and M2-type macrophages. 6-8 independent conditioned media were incubated with macrophages and the results are expressed relative to the mean of the expression of each of the markers in the control condition. No significant differences were observed between the three conditions (ANOVA test). *B:* Blood-derived human monocytes were incubated with 100 ng/ml LPS and 20 ng/ml INF-γ to induce M1 polarization, with 20 ng/ml IL-4 to induce M2 polarization, or with 24 h-conditioned medium (CM) from human adipocytes treated with nutlin (10 μM/48 h: CM nutlin) or doxorubicin (0.75 μg/ml for 4 h: CM doxo). The expression of the indicated surface markers for M0 (in black), M1 (blue), and M2 (green) were determined by flow cytometry analysis.

Supplemental Figure 4. Effect of doxorubicin and/or nutlin-3 in human adipocytes on insulin-induced glucose transport, insulin signaling, and lipolysis

A-B: Deoxyglucose (DOG) uptake in human adipocytes treated with 0.75 µg/ml doxorubicin for 24 h (*A*) or 10 µM Nutlin for 48 h (*B*) and stimulated with the indicated concentrations of insulin for 10 min. Data represent means ± SEM of 3 independent experiments with * p <0.05, ** p <0.01, *** p <0.001 control versus nutlin- or doxorubicin-treated cells. *C*: Human adipocytes were treated with 0.75 µg/ml doxorubicin for 24 h and incubated without or with insulin (ins, 0.5 nM) for 10 min. Western blot analysis of the expression of the indicated protein. Representative immunoblots and means ± SEM of 3 independent experiments are shown. Normalization was performed by quantifying ERK amount in each of the experiments. Data are expressed as percentage of insulin effect in untreated cells stimulated with insulin. *** $p < 0.001$ untreated cells stimulated with insulin *vs* doxorubicin-treated cells stimulated with insulin. *D*: Human adipocytes were treated with 10 µM nutlin for 48 h and incubated without or with insulin (ins, 0.5 nM) for 10 min before western blot analysis of the indicated proteins. A presentative immunoblot is shown and experiment was reproduced once with similar results. *E-F*: Glycerol production by human adipocytes treated with 0.75 µg/ml doxorubicin for 24 h (*C*) or 10 µM nutlin-3 for 48 h (*D*) as an index of lipolysis. Data are means ± SEM of 3 independent experiments with ** $p < 0.01$ control versus nutlin- or doxorubicin-treated cells

Supplemental Figure 5. p53 silencing partly prevents the inhibitory action of doxorubicin on insulin signaling

A: Western blot analysis of pThr308-PKB and total PKB in 3T3-L1 adipocytes transfected with control siRNA (si Ctrl) or siRNA against p53 (si p53) and incubated without (control) or with doxorubicin (doxo, 0.5 µg/ml) or nutlin-3 (10 µM) for 24 h or 48 h respectively before insulin stimulation (ins, 0.5 nM) for 10 min. Data are means ± SEM of 3 independent experiments and are expressed as % of insulin effect in control cells treated with si Ctrl. * $p <$ 0.05, ** p <0.01, *** $p < 0.001$ doxorubicin-treated cells versus control cells; $^{\#}p < 0.05$, $^{\#\#}p$

< 0.01, si Ctrl doxorubicin-treated cells *vs* si p53 doxorubicin-treated cells. *B*: Quantification of the ratio of pThr308-PKB/PKB corresponding to the western blots of Figures 7*D* and *E*. Graphs represent mean ± SEM of 3 independent experiments for doxorubicin and mean ± SE of 2 independent one for nutlin. ** p <0.01, doxorubicin-treated cells *vs* control cells.

Supplemental Figure 6. Schematic representation of the consequences of obesity-induced DNA damage in adipocytes.

ROS production by the AT and adipocytes is increased at the onset of obesity and is accompanied by an increase in DNA damage in adipocytes. The induction of DNA damage in adipocytes induces adipocyte insulin resistance, an increase in its lypolytic activity, and a chemotactic secretome for neutrophil and macrophage. These changes, also observed in obese AT, may trigger a deleterious cross-talk between adipocytes and immune cells leading to AT inflammation and metabolic dysfunctions.

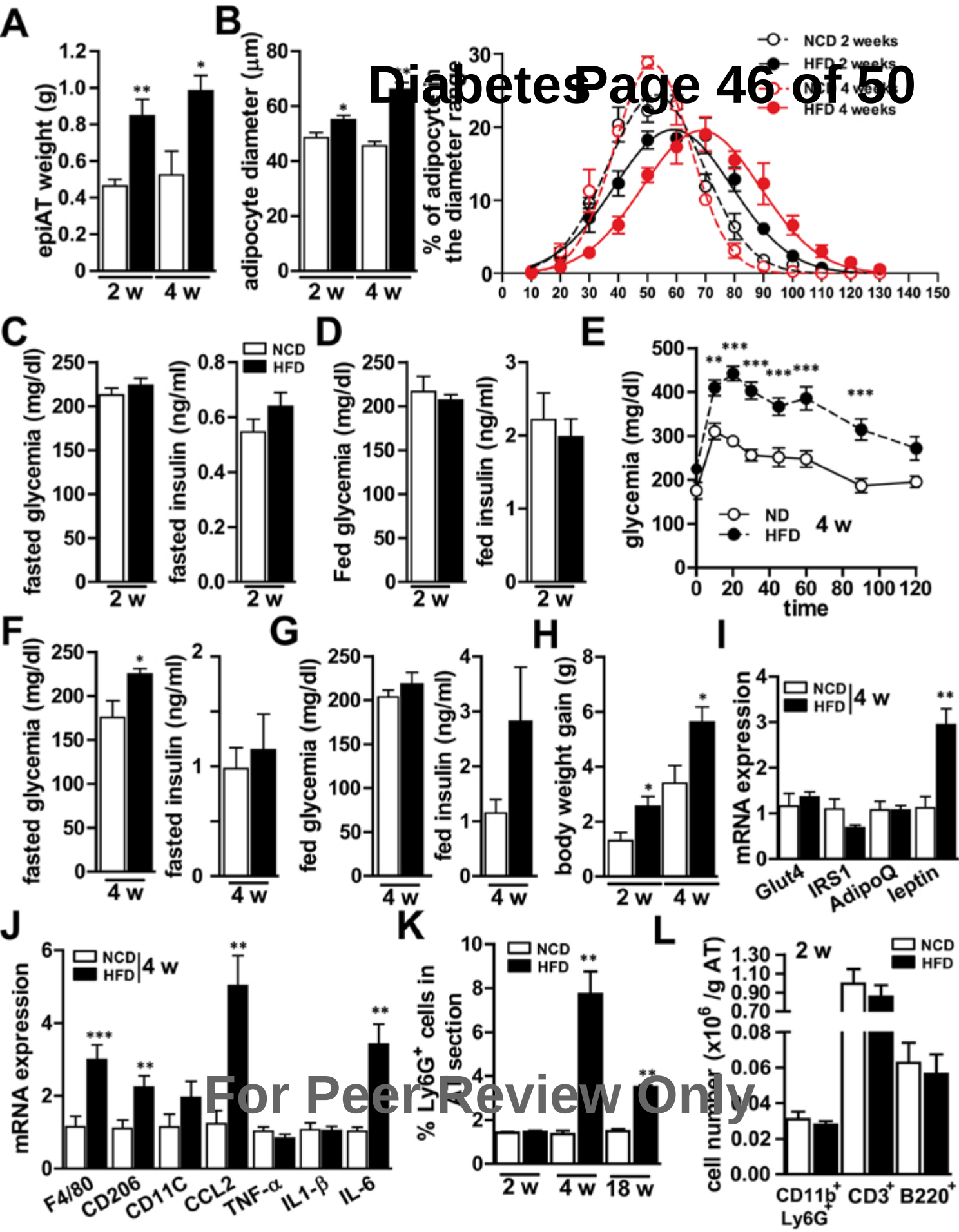

Supplemental Figure 1

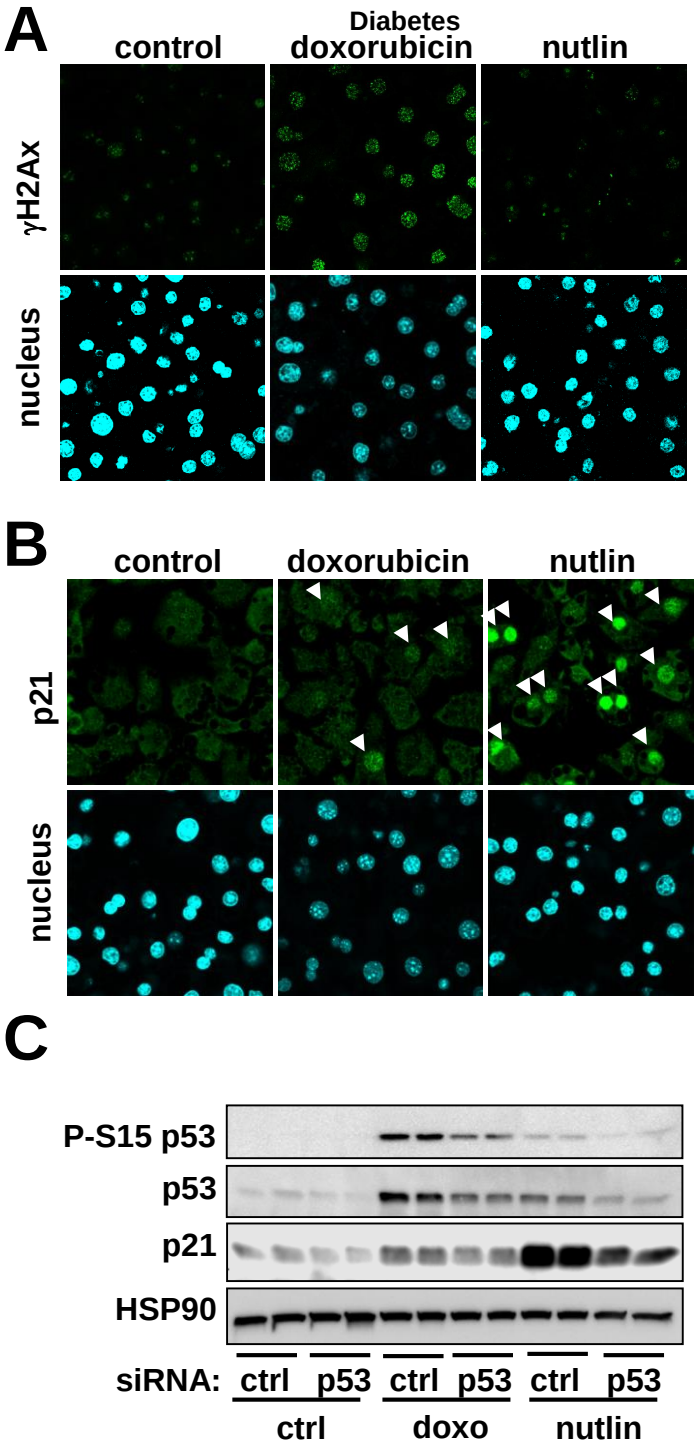

Supplemental Figure 2

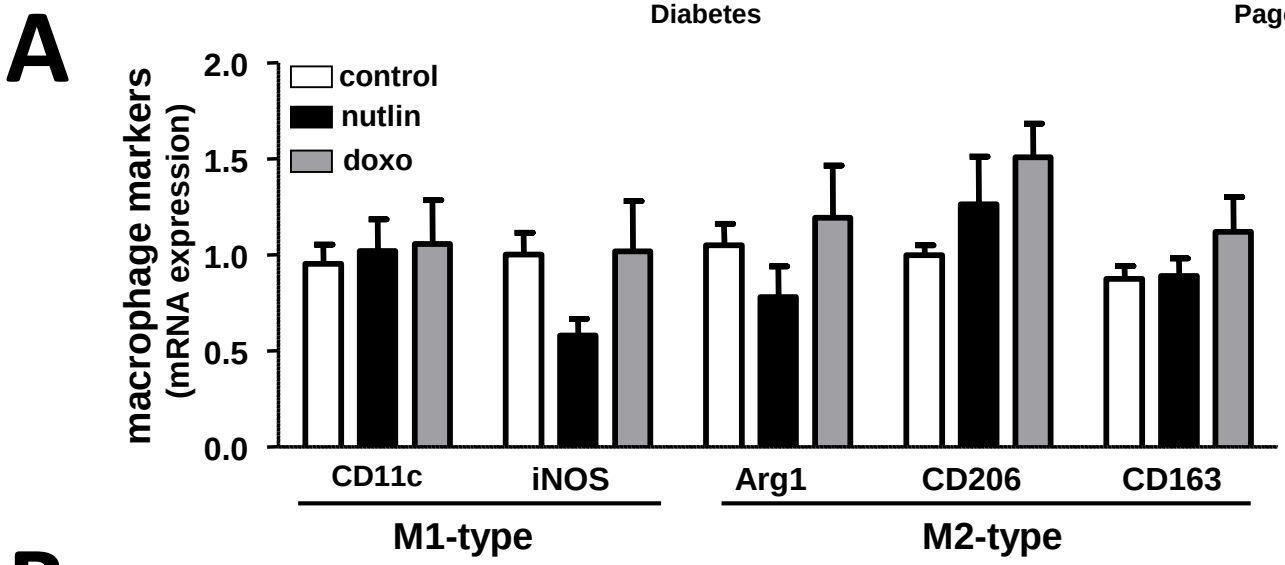

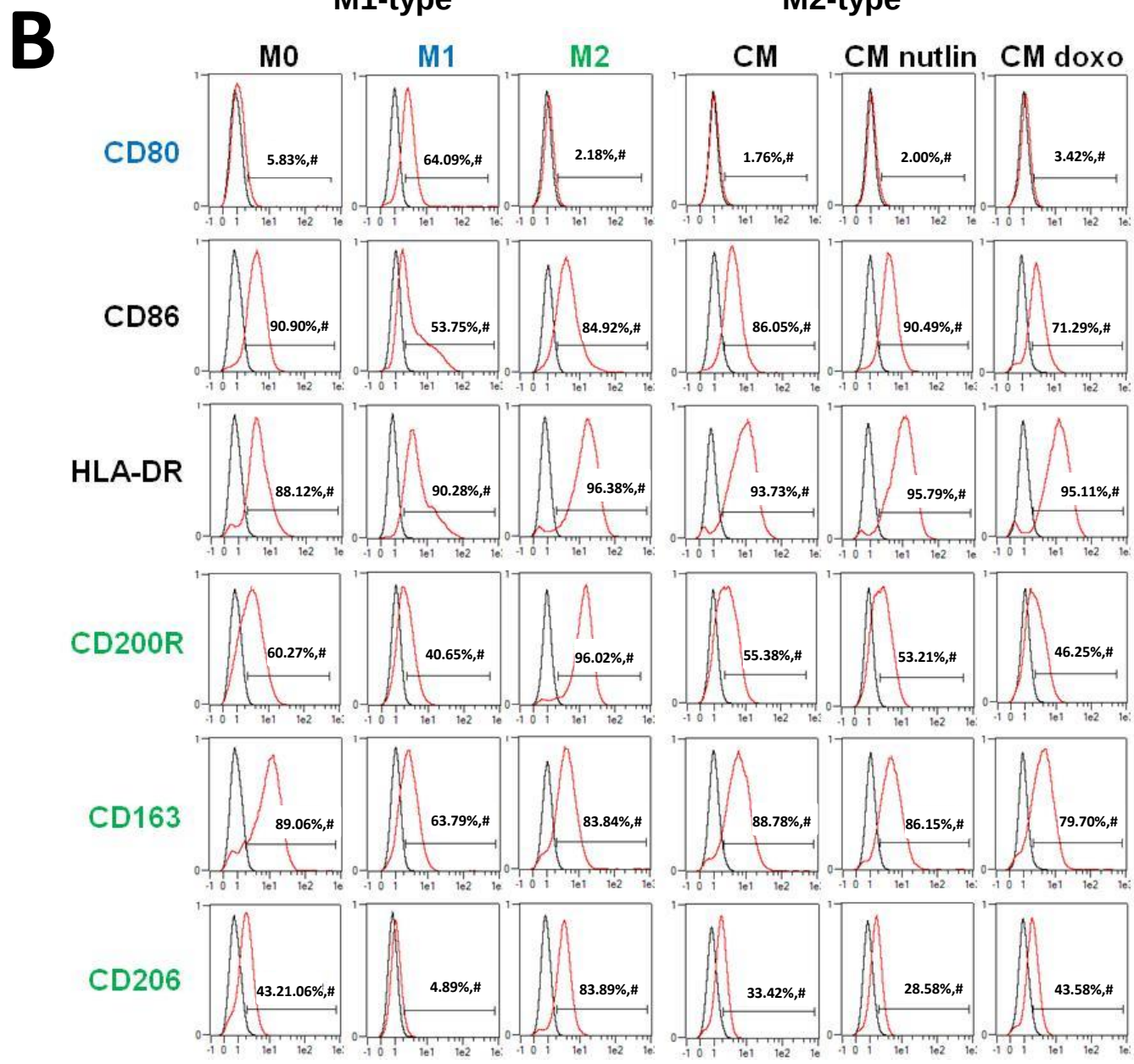

Supplemental figure 3

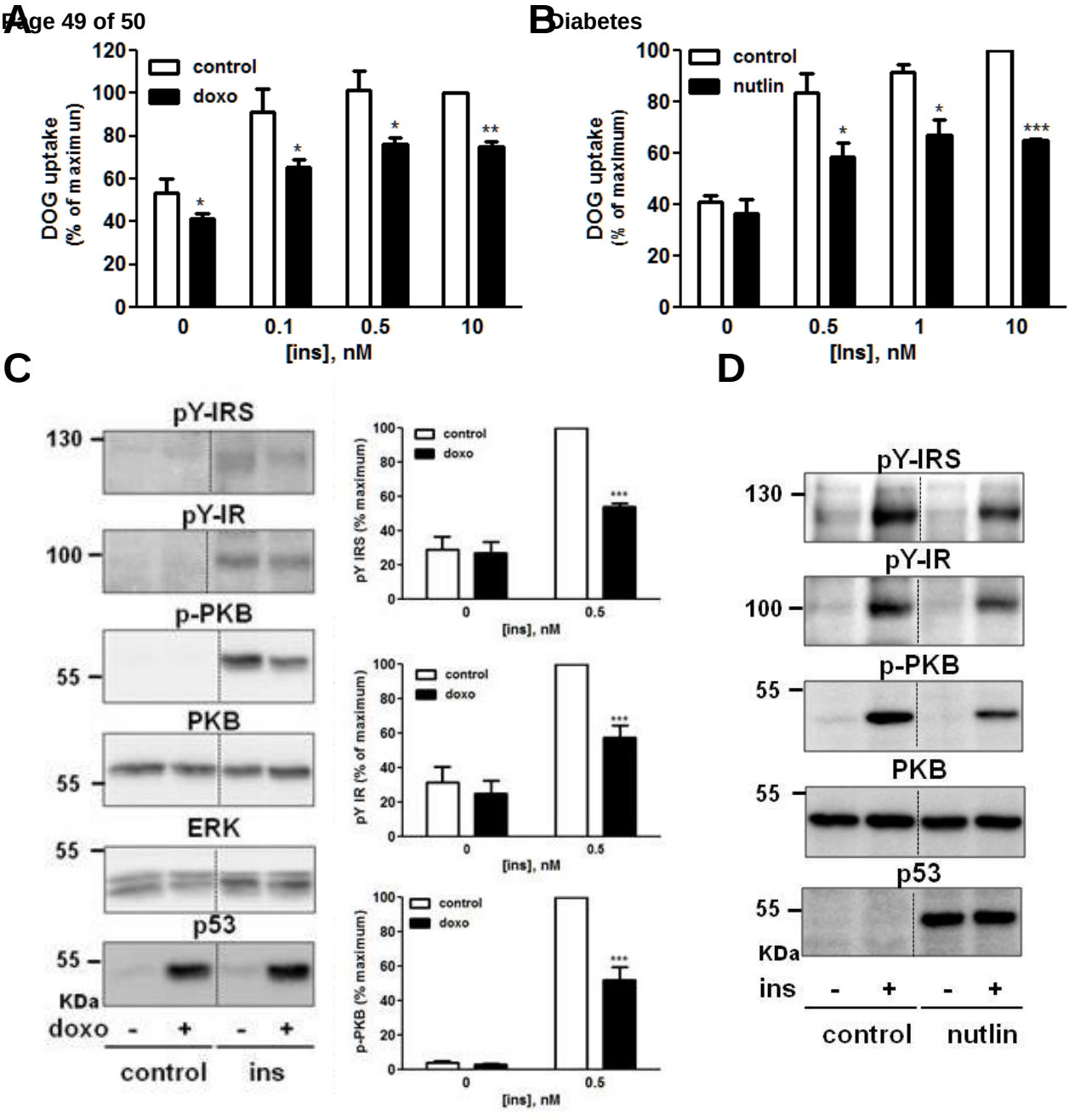

Supplemental figure 4

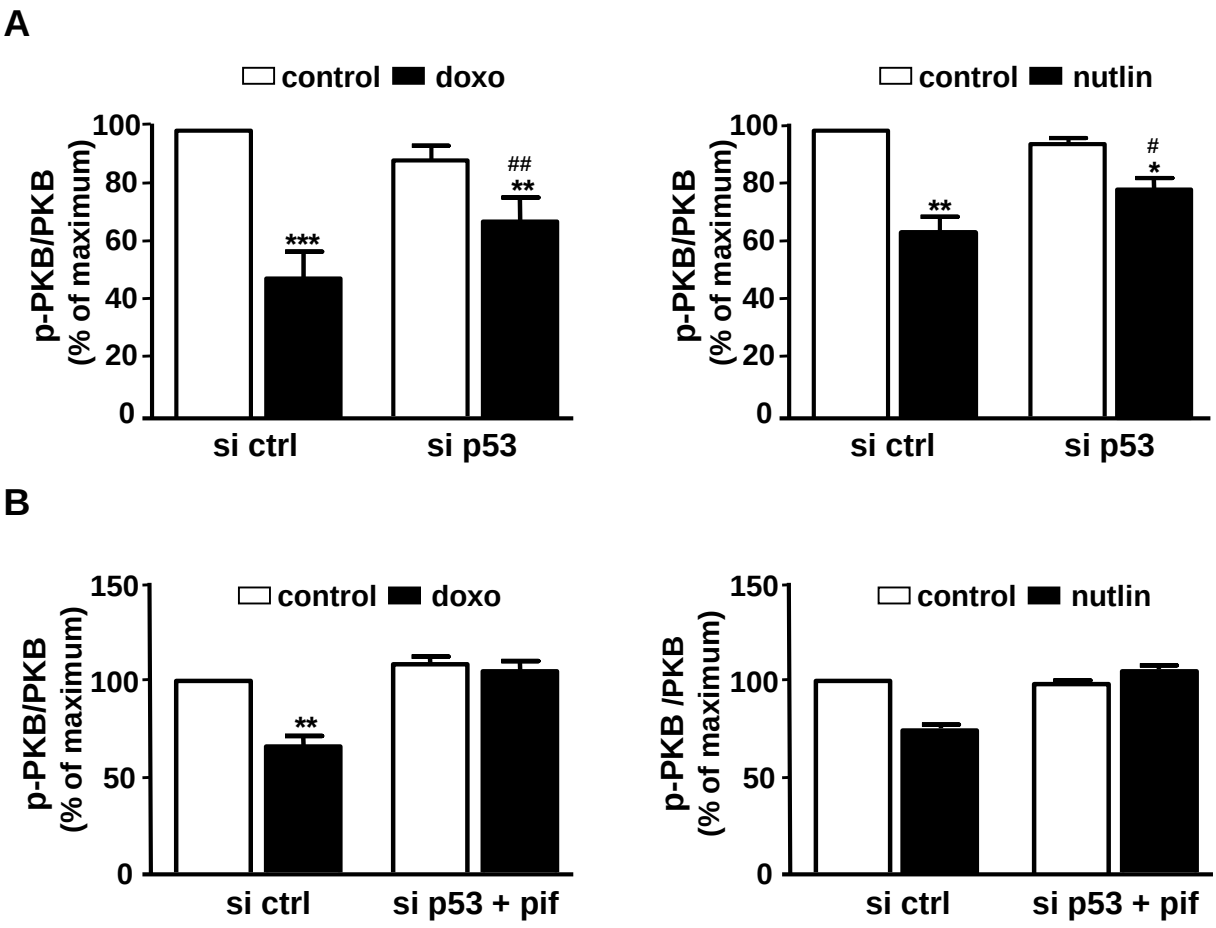

Supplemental Figure 5

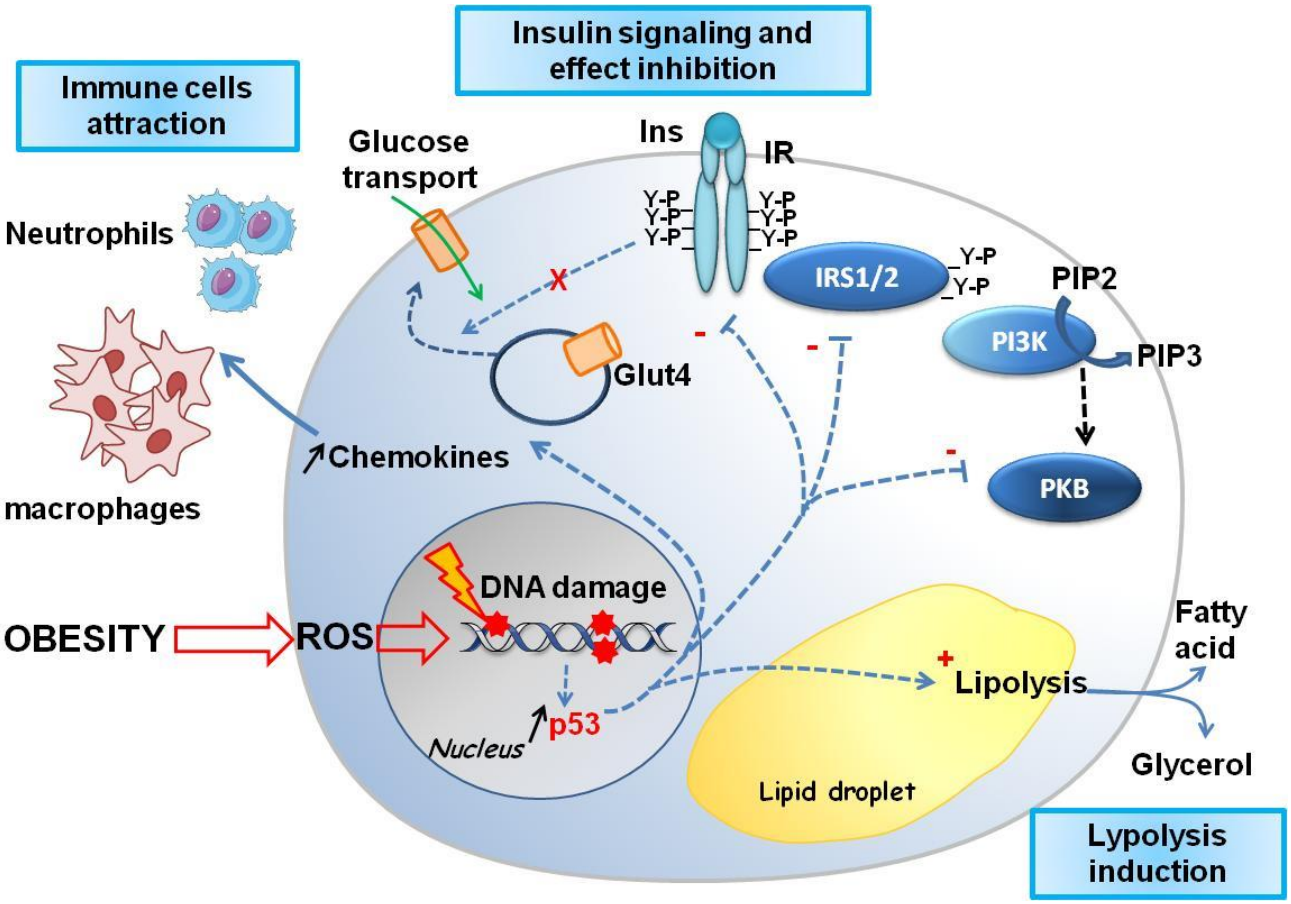

Supplemental Figure 6